

國立臺灣大學理學院應用物理研究所

碩士論文

Graduate Institute of Applied Physics

College of Science

National Taiwan University

Master Thesis



使用熱輔助佔據密度泛函理論對融合薁並苯之電子性
質的理論研究

Theoretical studies of electronic properties of fused azulene-acene
using thermally-assisted-occupation density functional theory

陳昱廷

Yu-Ting Chen

指導教授：蔡政達 博士

Advisor: Jeng-Da Chai, Ph.D.

中華民國 111 年 9 月

September, 2022



致謝



首先我要感謝指導教授蔡政達教授，在相關課程跟討論的時候提供我相關的知識跟建議，除了提供我研究的材料，也讓我嘗試計算自己設計的分子，並且對這篇論文提供許多指導。同時感謝口試委員林倫年主任以及張秀華教授對這篇論文不足之處提出建議，使本篇論文更加完整。我也要感謝家人提供我經濟上的援助，間接幫助這篇我完成這篇論文。還有許多同學及朋友，在無助的時候給我心理上的支持。

摘要



本論文使用熱輔助佔據密度泛函理論 (thermally-assisted-occupation density functional theory, TAO-DFT) 在局部密度近似 (local density approximation, LDA) 下研究融合奠並苯 (fused azulene-acene) 系統的電子性質，並與其同分異構物並苯 (acenes) 比較。若使用孔沈密度泛函理論 (Kohn-Sham density functional theory, KS-DFT) 計算融合奠並苯系統，會產生因其強關聯 (strongly correlated) 特性而發生的靜態關聯誤差 (static correlation error, SCE)，得到物理上不正確的三重態基態 (triplet ground state)。另一方面，孔沈密度泛函理論的計算過程中容易收斂到局域最小值，因此必須用大量初始條件和算法才能得到全域最小值，相較之下熱輔助佔據密度泛函理論能有效收斂到絕對最小值且修正靜態關聯誤差，同樣的計算資源下更有效率，因此本篇論文使用熱輔助佔據密度泛函理論來研究融合奠並苯系統的電子性質。

在短鏈 ($n < 8$) 融合奠並苯系統中使用基於孔沈密度泛函的混成泛函 B3LYP 得到負的單重態三重態能量差 (Singlet-Triplet gap)，而使用熱輔助佔據 B3LYP 的計算結果皆為正，也就是單重態基態。在局部密度近似下，長鏈 ($n < 75$) 的融合奠並苯的單重態三重態能量差皆小於並苯的能量差，得知兩端融合七五環可以將其降低，且減少幅度隨著長度增加而減少。從對稱馮諾伊曼熵 (symmetrized von Neumann entropy) 和軌域佔據數可以得知融合奠並苯的多重參考性 (multi-reference)，且從對稱馮諾伊曼熵對於鏈長的關係發現融合奠並苯與並苯斜率相同向上平移，發現融合奠並苯的軌域佔據數結構與並苯的類似。

關鍵字：融合奠並苯、並苯、熱輔助佔據密度泛函理論、強關聯系統

Abstract



In this thesis, we investigate the electronic properties of fused azulene-acene system using thermally-assisted-occupation density functional theory (TAO-DFT) in local density approximation (LDA) and compare to the properties of its isomer, acenes. If we use Kohn-Sham density functional theory (KS-DFT) to calculate, we get unphysical triplet ground state because of static correlation error (SCE) causing by the strong correlated (SC) character of fused azulene-acene. On the other hand, the energy usually truncate to local minimum during the iterating process of KS-DFT, and thus it needs lots of initial guess and algorithm to find the global minimum. TAO-DFT can effectively truncate to global minimum and correct SCE under the same computational resource, therefore is used to calculate the properties of fuse azulene-acene.

Negative singlet-triplet energy gap is obtained using hybrid functional B3LYP based on KS-DFT for fused azulene-acene in short length ($n < 8$). The result is positive, namely siglet ground state, using TAO-B3LYP. In LDA, singlet-triplet gaps of fused azulene-acene are all lower than ones of acenes. We can know that fusing the 7, 5 rings will lower ST gap, and the degree of reduction decrease as the length increase. Symmetrized von Neumann entropy and orbital occupation numbers show the multi-reference character of fused azulene-acene. The slope of fused azulene-acene of symmetrized von Neumann entropy to length is the same as one of acenes and translate upward, which indicates fused azulene-acene has similar structure of orbital occupation numbers to acenes.

Keywords: fused azulene-acene, acenes, thermally-assisted-occupation density functional theory, strong correlated system

Contents



致謝	ii
摘要	iii
Abstract	iv
Contents	v
List of Figures	vii
List of Tables.....	xiii
Chapter 1 Introduction	1
Chapter 2 Theoretical background	
2.1 Density functional theory.....	5
2.2 Hohenberg-Kohn theorems	8
2.3 Kohn-Sham method	10
2.4 Thermally-Assisted-Occupation density functional theory	14
2.5 Computational Details	17
Chapter 3 Results	20
Chapter 4 Concusion.....	35

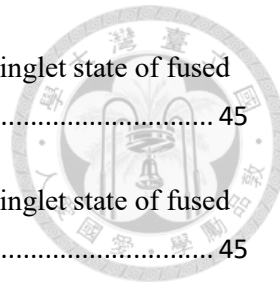


Chapter 5 Reference.....	36
Appendix A: Active orbital occupation numbers for the lowest singlet states of fused azulene-acene	42
Appendix B: Figures of real-space representation of HOMOs and LUMOs for the lowest singlet states of fused azulene-acene calculated using spin-restricted TAO-LDA($\theta = 7$ mHartree) at isovalue = 0.02 eV/Å³	45

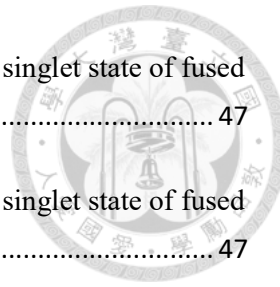
List of Figures



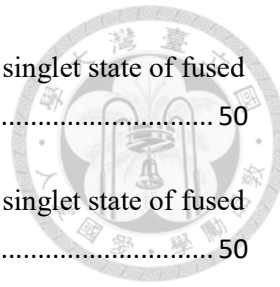
1.1: The structures of (a) n-acenes, (b) azulene and (c) fuse azulene-acene.....	2
3.1: Four kinds of singlet-triplet energy gaps of fused-azulene-acene, calculated by B3LYP and TAO-B3LYP ($\theta = 17.4$ mHartree)/6-31G* and reference data [12].	21
3.2: Singlet-triplet energy gap of acenes and fused azulene-acenes calculated by TAO-LDA ($\theta = 7$ mHartree)/6-31G* and TAO-B3LYP ($\theta = 17.4$ mHartree)/6-31G*.....	22
3.3: Singlet-triplet energy gap of fused azulene-acenes for n from 3 to 46 calculated by TAO-LDA ($\theta = 7$ mHartree)/6-31G* and for n from 3 to 75 calculated by TAO-LDA ($\theta = 7$ mHartree)/6-31G.....	25
3.4: Singlet-triplet energy gap for the longer acenes [13] and fused azulene-acenes calculated by TAO-LDA ($\theta = 7$ mHartree)/6-31G.....	26
3.5: Active orbital occupation numbers (HOMO-13, ..., HOMO-1, HOMO, LUMO, LUMO-1, ..., and LUMO-13) as a function of the fused azulene-acene length calculated using spin-restricted TAO-LDA ($\theta = 7$ mHartree)/6-31G.....	28
3.6: Symmetrized von Neumann entropy for the lowest singlet state of fused azulene-acenes and acenes calculated using spin-restricted TAO-LDA ($\theta = 7$ mHartree)/6-31G.....	29
3.7: Real-space representation of HOMO (left) and LUMO (right) for the singlet state of fused azulene-acene (n=3) with their occupation number 1.8157 and 0.1841.....	32
3.8: Real-space representation of HOMO (left) and LUMO (right) for the singlet state of fused azulene-acene (n=4) with their occupation number 1.3877 and 0.6119.....	32
3.9: Real-space representation of HOMO (left) and LUMO (right) for the singlet state of fused azulene-acene (n=5) with their occupation number 1.1038 and 0.8961.....	33
3.10: Real-space representation of HOMO (left) and LUMO (right) for the singlet state of fused azulene-acene (n=6) with their occupation number 1.0707 and 0.9301.....	33
3.11: Differences between STgap of n-acenes [13] and fused azulene-acene and dipole moment difference between single and triplet state of fused azulene-acene calculating using spin-unrestricted TAO-LDA ($\theta = 7$ mHartree)/6-31G.....	34



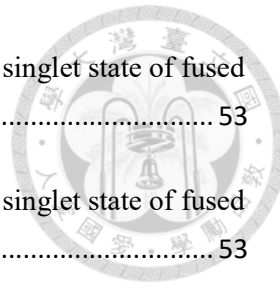
B.1: Real-space representation of HOMO (left) and LUMO (right) for the singlet state of fused azulene-acene (n=7) with their occupation number 1.1880 and 0.8147.....	45
B.2: Real-space representation of HOMO (left) and LUMO (right) for the singlet state of fused azulene-acene (n=8) with their occupation number 1.2742 and 0.7320.....	45
B.3: Real-space representation of HOMO (left) and LUMO (right) for the singlet state of fused azulene-acene (n=9) with their occupation number 1.3406 and 0.6694.....	45
B.4: Real-space representation of HOMO (left) and LUMO (right) for the singlet state of fused azulene-acene (n=10) with their occupation number 1.3927 and 0.6203.....	45
B.5: Real-space representation of HOMO (left) and LUMO (right) for the singlet state of fused azulene-acene (n=11) with their occupation number 1.4323 and 0.5825.....	45
B.6: Real-space representation of HOMO (left) and LUMO (right) for the singlet state of fused azulene-acene (n=12) with their occupation number 1.4628 and 0.5529.....	46
B.7: Real-space representation of HOMO (left) and LUMO (right) for the singlet state of fused azulene-acene (n=13) with their occupation number 1.4257 and 0.5668.....	46
B.8: Real-space representation of HOMO (left) and LUMO (right) for the singlet state of fused azulene-acene (n=14) with their occupation number 1.3102 and 0.6857.....	46
B.9: Real-space representation of HOMO (left) and LUMO (right) for the singlet state of fused azulene-acene (n=15) with their occupation number 1.2068 and 0.7927.....	46
B.10: Real-space representation of HOMO (left) and LUMO (right) for the singlet state of fused azulene-acene (n=16) with their occupation number 1.1160 and 0.8871.....	46
B.11: Real-space representation of HOMO (left) and LUMO (right) for the singlet state of fused azulene-acene (n=17) with their occupation number 1.0372 and 0.9693.....	46
B.12: Real-space representation of HOMO (left) and LUMO (right) for the singlet state of fused azulene-acene (n=18) with their occupation number 1.0405 and 0.9688.....	46
B.13: Real-space representation of HOMO (up) and LUMO (down) for the singlet state of fused azulene-acene (n=19) with their occupation number 1.1018 and 0.9099.....	47
B.14: Real-space representation of HOMO (up) and LUMO (down) for the singlet state of fused azulene-acene (n=20) with their occupation number 1.1547 and 0.8589.....	47



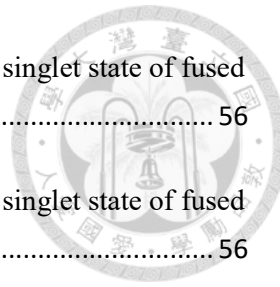
B.15: Real-space representation of HOMO (up) and LUMO (down) for the singlet state of fused azulene-acene (n=21) with their occupation number 1.2006 and 0.8146.....	47
B.16: Real-space representation of HOMO (up) and LUMO (down) for the singlet state of fused azulene-acene (n=22) with their occupation number 1.2405 and 0.7761.....	47
B.17: Real-space representation of HOMO (up) and LUMO (down) for the singlet state of fused azulene-acene (n=23) with their occupation number 1.2752 and 0.7426.....	48
B.18: Real-space representation of HOMO (up) and LUMO (down) for the singlet state of fused azulene-acene (n=24) with their occupation number 1.2782 and 0.7158.....	48
B.19: Real-space representation of HOMO (up) and LUMO (down) for the singlet state of fused azulene-acene (n=25) with their occupation number 1.2165 and 0.7807.....	48
B.20: Real-space representation of HOMO (up) and LUMO (down) for the singlet state of fused azulene-acene (n=26) with their occupation number 1.1593 and 0.8409.....	48
B.21: Real-space representation of HOMO (up) and LUMO (down) for the singlet state of fused azulene-acene (n=27) with their occupation number 1.1063 and 0.8967.....	49
B.22: Real-space representation of HOMO (up) and LUMO (down) for the singlet state of fused azulene-acene (n=28) with their occupation number 1.0577 and 0.9478.....	49
B.23: Real-space representation of HOMO (up) and LUMO (down) for the singlet state of fused azulene-acene (n=29) with their occupation number 1.0131 and 0.9948.....	49
B.24: Real-space representation of HOMO (up) and LUMO (down) for the singlet state of fused azulene-acene (n=30) with their occupation number 1.0379 and 0.9721.....	49
B.25: Real-space representation of HOMO (up) and LUMO (down) for the singlet state of fused azulene-acene (n=31) with their occupation number 1.0772 and 0.9347.....	49
B.26: Real-space representation of HOMO (up) and LUMO (down) for the singlet state of fused azulene-acene (n=32) with their occupation number 1.1131 and 0.9004.....	50
B.27: Real-space representation of HOMO (up) and LUMO (down) for the singlet state of fused azulene-acene (n=33) with their occupation number 1.1461 and 0.8690.....	50
.....	50



B.29: Real-space representation of HOMO (up) and LUMO (down) for the singlet state of fused azulene-acene (n=35) with their occupation number 1.2038 and 0.8138.....	50
B.30: Real-space representation of HOMO (up) and LUMO (down) for the singlet state of fused azulene-acene (n=36) with their occupation number 1.1789 and 0.8195.....	50
B.31: Real-space representation of HOMO (up) and LUMO (down) for the singlet state of fused azulene-acene (n=37) with their occupation number 1.1394 and 0.8614.....	51
B.32: Real-space representation of HOMO (up) and LUMO (down) for the singlet state of fused azulene-acene (n=38) with their occupation number 1.1021 and 0.9008.....	51
B.33: Real-space representation of HOMO (up) and LUMO (down) for the singlet state of fused azulene-acene (n=39) with their occupation number 1.0669 and 0.9380.....	51
B.34: Real-space representation of HOMO (up) and LUMO (down) for the singlet state of fused azulene-acene (n=40) with their occupation number 1.0339 and 0.9730.....	51
B.35: Real-space representation of HOMO (up) and LUMO (down) for the singlet state of fused azulene-acene (n=41) with their occupation number 1.0059 and 1.0027.....	51
B.36: Real-space representation of HOMO (up) and LUMO (down) for the singlet state of fused azulene-acene (n=42) with their occupation number 1.0367 and 0.9736.....	52
B.37: Real-space representation of HOMO (up) and LUMO (down) for the singlet state of fused azulene-acene (n=43) with their occupation number 1.0657 and 0.9462.....	52
B.38: Real-space representation of HOMO (up) and LUMO (down) for the singlet state of fused azulene-acene (n=44) with their occupation number 1.0928 and 0.9204.....	52
B.39: Real-space representation of HOMO (up) and LUMO (down) for the singlet state of fused azulene-acene (n=45) with their occupation number 1.1182 and 0.8963.....	52
B.40: Real-space representation of HOMO (up) and LUMO (down) for the singlet state of fused azulene-acene (n=46) with their occupation number 1.1420 and 0.8737.....	52
B.41: Real-space representation of HOMO (up) and LUMO (down) for the singlet state of fused azulene-acene (n=47) with their occupation number 1.1586 and 0.8523.....	53
B.42: Real-space representation of HOMO (up) and LUMO (down) for the singlet state of fused azulene-acene (n=48) with their occupation number 1.1286 and 0.8725.....	53



B.43: Real-space representation of HOMO (up) and LUMO (down) for the singlet state of fused azulene-acene (n=49) with their occupation number 1.0998 and 0.9031.....	53
B.44: Real-space representation of HOMO (up) and LUMO (down) for the singlet state of fused azulene-acene (n=50) with their occupation number 1.0723 and 0.9323.....	53
B.45: Real-space representation of HOMO (up) and LUMO (down) for the singlet state of fused azulene-acene (n=51) with their occupation number 1.0460 and 0.9601.....	53
B.46: Real-space representation of HOMO (up) and LUMO (down) for the singlet state of fused azulene-acene (n=52) with their occupation number 1.0211 and 0.9866.....	54
B.47: Real-space representation of HOMO (up) and LUMO (down) for the singlet state of fused azulene-acene (n=53) with their occupation number 1.0119 and 0.9972.....	54
B.48: Real-space representation of HOMO (up) and LUMO (down) for the singlet state of fused azulene-acene (n=54) with their occupation number 1.0360 and 0.9745.....	54
B.49: Real-space representation of HOMO (up) and LUMO (down) for the singlet state of fused azulene-acene (n=55) with their occupation number 1.0588 and 0.9529.....	54
B.50: Real-space representation of HOMO (up) and LUMO (down) for the singlet state of fused azulene-acene (n=56) with their occupation number 1.0806 and 0.9323.....	54
B.51: Real-space representation of HOMO (up) and LUMO (down) for the singlet state of fused azulene-acene (n=57) with their occupation number 1.1013 and 0.9127.....	55
B.52: Real-space representation of HOMO (up) and LUMO (down) for the singlet state of fused azulene-acene (n=58) with their occupation number 1.1210 and 0.8941.....	55
B.53: Real-space representation of HOMO (up) and LUMO (down) for the singlet state of fused azulene-acene (n=59) with their occupation number 1.1217 and 0.8797.....	55
B.54: Real-space representation of HOMO (up) and LUMO (down) for the singlet state of fused azulene-acene (n=60) with their occupation number 1.0983 and 0.9046.....	55
B.55: Real-space representation of HOMO (up) and LUMO (down) for the singlet state of fused azulene-acene (n=61) with their occupation number 1.0757 and 0.9286.....	55
B.56: Real-space representation of HOMO (up) and LUMO (down) for the singlet state of fused azulene-acene (n=62) with their occupation number 1.0540 and 0.9517.....	56



B.57: Real-space representation of HOMO (up) and LUMO (down) for the singlet state of fused azulene-acene (n=63) with their occupation number 1.0331 and 0.9740.....	56
B.58: Real-space representation of HOMO (up) and LUMO (down) for the singlet state of fused azulene-acene (n=64) with their occupation number 1.0130 and 0.9953.....	56
B.59: Real-space representation of HOMO (up) and LUMO (down) for the singlet state of fused azulene-acene (n=65) with their occupation number 1.0159 and 0.9936.....	56
B.60: Real-space representation of HOMO (up) and LUMO (down) for the singlet state of fused azulene-acene (n=66) with their occupation number 1.0355 and 0.9750.....	56
B.61: Real-space representation of HOMO (up) and LUMO (down) for the singlet state of fused azulene-acene (n=67) with their occupation number 1.0545 and 0.9572.....	56
B.62: Real-space representation of HOMO (up) and LUMO (down) for the singlet state of fused azulene-acene (n=68) with their occupation number 1.0726 and 0.9401.....	57
B.63: Real-space representation of HOMO (up) and LUMO (down) for the singlet state of fused azulene-acene (n=69) with their occupation number 1.0900 and 0.9236.....	57
B.64: Real-space representation of HOMO (up) and LUMO (down) for the singlet state of fused azulene-acene (n=70) with their occupation number 1.1068 and 0.9078.....	57
B.65: Real-space representation of HOMO (up) and LUMO (down) for the singlet state of fused azulene-acene (n=71) with their occupation number 1.0972 and 0.9057.....	57
B.66: Real-space representation of HOMO (up) and LUMO (down) for the singlet state of fused azulene-acene (n=72) with their occupation number 1.0781 and 0.9261.....	57
B.67: Real-space representation of HOMO (up) and LUMO (down) for the singlet state of fused azulene-acene (n=73) with their occupation number 1.0595 and 0.9458.....	57
B.68: Real-space representation of HOMO (up) and LUMO (down) for the singlet state of fused azulene-acene (n=74) with their occupation number 1.0416 and 0.9649.....	57
B.69: Real-space representation of HOMO (up) and LUMO (down) for the singlet state of fused azulene-acene (n=75) with their occupation number 1.0242 and 0.9834.....	58



List of Tables

3.1: The unrestricted singlet (US), unrestricted triplet (UT), restricted singlet (RS) and restricted triplet (RT) state energy of fused-azulene-acene calculated by B3LYP/6-31G* are given in Hartrees. The four kind of singlet-triplet energy gaps are in kcal/mol.	20
3.2: The unrestricted singlet (US) and unrestricted triplet (UT) energy of fused-azulene-acene calculated by TAO-LDA ($\theta = 7$ mHartree)/6-31G* are given in Hartrees. The ST gaps are given in kcal/mol.....	22
3.3: The unrestricted singlet (US) and unrestricted triplet (UT) energy of fused-azulene-acene calculated by TAO-B3LYP ($\theta = 17.4$ mHartree)/6-31G* are given in Hartrees. The ST gaps are given in kcal/mol. The restricted singlet (RS) state energy and the energy difference between RS and US (RS-US) are also listed in Hartrees in comparison.....	23
3.4: The unrestricted singlet (US) and unrestricted triplet (UT) energy of linear acenes calculated by TAO-LDA ($\theta = 7$ mHartree)/6-31G* are given in Hartrees. The ST gaps are given in kcal/mol.....	23
3.5: The unrestricted singlet (US) and unrestricted triplet (UT) energy of linear acenes calculated by TAO-B3LYP ($\theta = 17.4$ mHartree)/6-31G* are given in Hartrees. The ST gaps are given in kcal/mol.	24
3.6: The unrestricted singlet (US) and unrestricted triplet (UT) energy of fused-azulene-acene and acenes calculated by TAO-LDA ($\theta = 7$ mHartree)/6-31G* are given in Hartrees. The ST gaps of both fused-azulene-acene and acene are given in kcal/mol.....	26
3.7: The unrestricted singlet (US) and the unrestricted triplet (UT) energy of fused azulene-acenes calculated by TAO-LDA ($\theta = 7$ mHartree)/6-31G are given in Hartrees. The ST gaps of fused azulene-acene, acenes [13] and Δ are given in kcal/mol where Δ is the difference between ST gaps of fused azulene-acene and acenes. The dipole moment of US and UT and the singlet-triplet dipole moment gap are given in debye. The symmetrized von Neumann entropy of both fused azulene-acene and acenes [13] are given.	30
A: Active orbital occupation numbers (HOMO-13, ..., HOMO-1, LUMO-1, ..., LUMO-13) for the lowest singlet states of fused azulene-acene, calculated by spin-restricted TAO-LDA ($\theta = 7$ mHartree), using the 6-31G basis set.	42



Chapter 1

Introduction

Semiconductor is a type of materials has an electrical conductivity value falling between that of a conductor and an insulator. The fermi level usually falls between conduction band (CB) and valence band (VB), where charge carriers with enough thermal energy can be excited to CB or VB and diffuse or drift around. This kind of materials has various applications such as electronic, optical or spintronic devices [1][18].

In addition to traditional semiconductor materials, scientists are also interesting in organic electronic materials. One of the fascinating materials is graphene, which is discovered by Andre K. Geim and Konstatin S. Novoselov. Graphene is allotrope of carbon having 2D single layer atoms in honeycomb lattice. It has been researched extensively in decades due to its fascinating properties such as massless relativistic Dirac Fermion, non-zero minimum conductivity, room-temperature integer quantum Hall effect [2][29]. The high electron mobility and long spin lifetimes make graphene possible to be applied in constructing graphene-based electronics and spintronics devices [3]. All these outstanding properties of graphene are due to its two-dimensional monolayer of honeycomb lattice carbon structure, related to their π -conjugated bounding topology. However, gap opening between valence and conduction band makes graphene different from semiconductor silicon [30].



Acenes, one dimensional graphene nanoribbons (GNRs), which are formed linearly with benzene rings shown in Figure 1.1(a), have been studied widely owing to their tunable optical gaps. Lattice symmetry breaking and finite size effect produce bandgap in graphene [31][32]. Also, their singlet fission phenomenon has been observed and has several possible usages [4][5]. The electronic structure of acenes has been strongly debated. Some studies predict the existence of triplet ground state or the non-monotonicity of the decay in the singlet-triplet gap [6]. Due to the π -conjugated system, the static correlated effect is strong in density functional theory (DFT). Kohn-Sham DFT may not finely converge the single point energy to global minimum. High-level ab initio multireference method, such as the density matrix renormalization group (DMRG) algorithm [10], the variational two-electron reduced density matrix (2-RDM) method [11][32], can accurately describe the strong correlated effects. However, these methods can be extremely expensive for long-chained acenes. In contrast, thermally-assisted-occupation density functional theory (TAO-DFT) introduce the Fermi-Dirac distribution to approximate the natural orbital occupation numbers and an additional tunable parameter, a fictitious temperature θ . It can effectively reduce the computational cost and find the global minima more accurately.

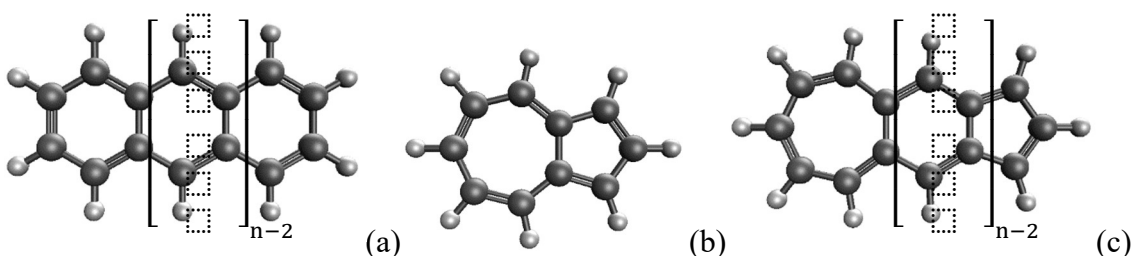
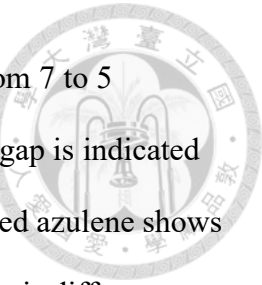


Figure 1.1: The structures of (a) n-acenes, (b) azulene and (c) fuse azulene-acene

Azulene is isomer of naphthalene, consisting of five and seven membered rings, which is shown in Figure 1.1 (b). Its singlet-triplet (ST) gap is lower than naphthalene



since it is less stable and the dipole moment of singlet state pointing from 7 to 5 membered ring. The reversed polarity of triplet state causing lower ST gap is indicated by Braid's theory of triplet state antiaromaticity [15][16]. Repeated fused azulene shows negative ST gap which means triplet ground state [19]. This observation is different from that of acenes and was predicted from the study using UB3LYP method [20]. The ground state crossover of singlet and triplet may be useful in tuning ST gap of acenes, where the system is designed as fused azulene-acene in Figure 1.1 (c).

Defects, such as line defects or edge defects, often appear during the synthesis of graphene. They can be applied in spin-filter devices [9]. Replacing the two ends of acenes by fused five or seven membered rings can be seen as the edge defects of acenes. Theoretically, the fused azulene-acene have lower ST gap than its isomer of acenes. As the length increase, the effect of the edge defect should be less relevant and the ST gap of the two should converge. Though there is a study of the fused azulene-acene system obtained the results of triplet ground state using UB3LYP geometries and multireference calculations optimizing which against our prediction [12].

In this thesis, we reproduce the result of triplet ground state by using B3LYP to optimize. In comparison, TAO local density approximation (TAO-LDA) and TAO-B3LYP are employing due to its computational efficiency and ability dealing with the strong correlated cases to generate the result similar to the long acenes [8][13][26][34], showing how five and seven membered rings reducing ST gap effectively in short length. In convenient, we define the length of fused azulene-acene with a number n which the molecular formula satisfies $C_{4n+2}H_{2n+4}$. Due to the expensive computational costs, we only obtain both spin-restricted and spin-unrestricted B3LYP results from 2 to 8 by assuming lots of initial guesses, and compare the results to triplet ground state references. From 2 to 20, we compute with both spin-unrestricted TAO-LDA and TAO-

B3LYP to see the differences between fused azulene-acene and linear acenes. Using TAO-LDA, the length can be calculated up to 75 without initial guesses and thus can be compared to the results of n-acenes, where the singlet-triplet energy gap, orbital occupation numbers, symmetrized von Neumann entropy and dipole moment are included. The electronic properties can provide information for further applications like defect controlling or spintronic devices.

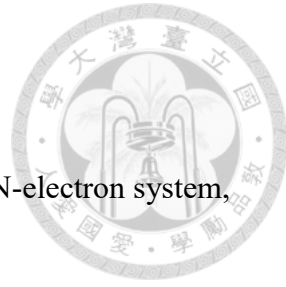


Chapter 2

Theoretical background

2.1 Density functional theory

Density functional theory (DFT) is a popular method widely used in physics, chemistry and materials science in recent years. Using this computational quantum mechanical modelling method, the electronic properties of a many-body systems are allowed to be determined. In many-body problem, the electronic structure is covered by Schrödinger's equation. The solution of this equation is a wave function with $3N$ spatial coordinates and usually cannot be solved. Due to the complexity solving it, one is interesting in reducing the variables from $3N$ to only 3 by representing system energies in electric density instead of electric wave functions. The roots of DFT is from the Thomas-Fermi model for the electronic structure of materials. DFT was first given a rigorous proof by Hohenberg and Kohn in 1964 [21]. The original Hohenberg-Kohn theorem describes that both the non-degenerated ground state density and ground state wave function have one to one relation with the system external potential. In 1965, Walter Kohn and Le Jeu Sham followed the Hohenberg-Kohn theorem and developed a practical and computable self-consistent method, which is called Kohn-Sham DFT [22]. In this theory, the many-body problem of interacting electrons in a static external potential is reduced to fictitious non-interacting electrons in an effective potential. Assuming a self-consistent initial condition, the solution of Kohn-Sham equation will converge by iterative process. Kohn-Sham theory puts the concept of DFT into practical calculations to deal with electronic structure, molecules binding energy, materials band



gap and so on.

To get the energy and the 3N-dimensional wave function of an N-electron system, one need to solve the Schrödinger equation

$$\hat{H}\Psi(\mathbf{x}_1, \dots, \mathbf{x}_N, \mathbf{R}_1, \dots, \mathbf{R}_N) = E\Psi(\mathbf{x}_1, \dots, \mathbf{x}_N, \mathbf{R}_1, \dots, \mathbf{R}_N) \quad (2.1.1)$$

where E is the electronic energy, Ψ is the wave function, \mathbf{x}_i is the coordinates of electron i comprising space coordinates \mathbf{r}_i and spin coordinates s_i and \hat{H} is the Hamiltonian operator which includes electronic kinetic energy, potential energy between electrons, nuclear kinetic energy, potential energy between nuclei, and potential energy between nuclei and electrons

$$\begin{aligned} \hat{H} = & \sum_{i=1}^N \left(\frac{1}{2} \nabla_i^2 \right) + \sum_{i=1}^N \sum_{i' < i} \frac{1}{|\mathbf{r}_i - \mathbf{r}_{i'}|} + \sum_{j=1}^M \left(\frac{1}{2m_j} \nabla_j^2 \right) + \sum_{j=1}^M \sum_{j' < j} \frac{Z_j Z_{j'}}{|\mathbf{R}_j - \mathbf{R}_{j'}|} \\ & - \sum_{i=1}^N \sum_{j=1}^M \frac{Z_j}{|\mathbf{r}_i - \mathbf{R}_j|} \end{aligned} \quad (2.1.2)$$

with N , M , \mathbf{r}_i , \mathbf{R}_j , m_j , Z_j being the amount of electrons, amount of nuclei, positions of electron i, position of nucleus j, mass of nucleus j and charge number of nucleus j.

In the Born-Oppenheimer nonrelativistic approximation, nuclei are way heavier than electrons and thus considered static. Then the nuclear kinetic energy can be ignored and the potential energy between nucleus can be seen as constant. The Hamiltonian can be simplified as

$$\hat{H} = \sum_{i=1}^N \left(\frac{1}{2} \nabla_i^2 \right) + \sum_{i=1}^N v(\mathbf{r}_i) + \sum_{i < j}^N \frac{1}{\mathbf{r}_{ij}} \quad (2.1.3)$$

$$= \hat{T} + \hat{V}_{ext} + \hat{V}_{ee} \quad (2.1.4)$$



in which

$$v(\mathbf{r}_i) = - \sum_{\alpha} \frac{Z_{\alpha}}{r_{i\alpha}} \quad (2.1.5)$$

is the external potential acting on electron i due to nuclei of charges Z_{α} . The wave function can simplified to a $3N$ variables function $\Psi(\mathbf{r}_1, \dots, \mathbf{r}_N)$.

To reach the goal of reducing $3N$ variables to 3, one wonders if it is possible to represent the system energies terms of electron density. The density function in terms of Ψ is

$$\rho(\mathbf{r}_1) = N \int \dots \int |\Psi(\mathbf{x}_1, \dots, \mathbf{x}_N)|^2 d\mathbf{x}_1 d\mathbf{x}_2 \dots d\mathbf{x}_N \quad (2.1.6)$$

which is a simple function of three spatial variables, integrating to the total number of electrons,

$$\int \rho(\mathbf{r}) d\mathbf{r} = N \quad (2.1.7)$$

The expectation value of external potential is a function of Ψ

$$\langle V_{ext} \rangle = V_{ext}[\Psi] = \langle \Psi | V_{ext} | \Psi \rangle = \int \dots \int \Psi^* V_{ext} \Psi d\mathbf{r}_1 \dots d\mathbf{r}_N \quad (2.1.8)$$

where V_{ext} is the external potential in (2.1.4). By (2.1.6), (2.1.8) can be simplified as a function of ρ

$$V_{ext}[\rho] = \int \rho(\mathbf{r}_1) V_{ext}(\mathbf{r}_1) d\mathbf{r}_1 \quad (2.1.9)$$

This process shows that we can represent external potential in terms of electron density without assumption. Though $T[\rho]$ and $V_{ee}[\rho]$ remain unknown. We can write energy functional as

$$E[\rho] = T[\rho] + V_{ee}[\rho] + \int \rho(\mathbf{r}_1) V_{ext}(\mathbf{r}_1) d\mathbf{r}_1$$

$$= F[\rho] + \int \rho(\mathbf{r}_1) V_{ext}(\mathbf{r}_1) d\mathbf{r}_1$$



where $F[\rho]$ is the same for all Hamiltonians of N-electron systems.

2.2 Hohenberg-Kohn theorems

For a nondegenerate ground-state N-electron system, the external potential V_{ext} fixes the Hamiltonian and thus N and V_{ext} determine ground state energy E_0 and ground state wave function Ψ_0 , and also ground state electron density ρ by definition. Hohenberg and Kohn in 1964 gave the 1st HK theorem which use electron density as basic variable to determine the external potential instead, showing the one to one relation between ground state electron density and external potential.

Suppose there are two different potential $V_{ext}^a(\mathbf{r})$ and $V_{ext}^b(\mathbf{r})$ with ground state wave functions Ψ^a and Ψ^b respectively having same density ρ . We have two Hamiltonians H^a , H^b , E_0^a and E_0^b accordingly. Taking Ψ^b as a trial function for the H^a , we would have

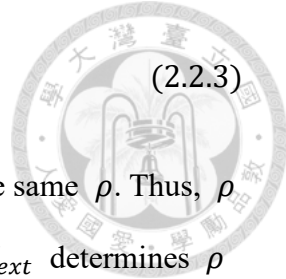
$$\begin{aligned} E_0^a &< \langle \Psi^b | H^a | \Psi^b \rangle = \langle \Psi^b | H^b | \Psi^b \rangle + \langle \Psi^b | H^a - H^b | \Psi^b \rangle \\ &= E_0^b + \int \rho(\mathbf{r}) [V_{ext}^a(\mathbf{r}) - V_{ext}^b(\mathbf{r})] d\mathbf{r} \end{aligned} \quad (2.2.1)$$

Taking Ψ^a as a trial function for the H^b , we have

$$\begin{aligned} E_0^b &< \langle \Psi^a | H^b | \Psi^a \rangle = \langle \Psi^a | H^a | \Psi^a \rangle + \langle \Psi^a | H^b - H^a | \Psi^a \rangle \\ &= E_0^a + \int \rho(\mathbf{r}) [V_{ext}^b(\mathbf{r}) - V_{ext}^a(\mathbf{r})] d\mathbf{r} \end{aligned} \quad (2.2.2)$$

Adding (2.2.1) and (2.2.2), we would obtain a contradict equation

$$E_0^a + E_0^b < E_0^b + E_0^a \quad (2.2.3)$$



There cannot be two different external potential V_{ext} giving the same ρ . Thus, ρ determines N and V_{ext} proved by the 1^{st} HK theorem; N and V_{ext} determines ρ by solving Schrödinger equation. Density ρ and external potential V_{ext} do have one to one relation.

The 2^{nd} HK theorem state that the energy functional gives the minimum energy if and only if the variable density is the ground state density. From the 1^{st} HK theorem, a density $\tilde{\rho}$ leads to its particular external potential \tilde{V}_{ext} , Hamiltonian \tilde{H} and wave function $\tilde{\Psi}$. Use a trial density $\tilde{\rho}$ which is different from ground state density ρ_0 with its own H as the input of energy functional, we have

$$E[\tilde{\rho}] = \langle \tilde{\Psi} | H | \tilde{\Psi} \rangle > \langle \Psi | H | \Psi \rangle = E[\rho_0] = E_0 \quad (2.2.4)$$

Assuming differentiability of $E[\tilde{\rho}]$, since (2.2.4) indicates that ground state energy satisfies stationary principle, we can apply variational principle with the constraint

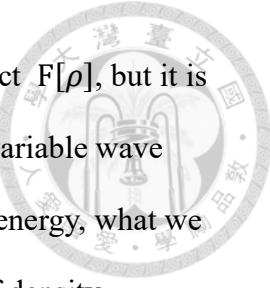
$$\int \rho(\mathbf{r}) d\mathbf{r} - N = 0$$

$$\delta\{E[\rho] - \mu[\int \rho(\mathbf{r}) d\mathbf{r} - N]\} = 0 \quad (2.2.5)$$

which provides the Euler-Lagrange equation

$$\mu = \frac{\delta E[\rho]}{\delta \rho(\mathbf{r})} = V_{ext}(\mathbf{r}) + \frac{\delta F[\rho]}{\rho(\mathbf{r})} \quad (2.2.6)$$

The quantity μ is not only a Lagrange multiplier but also chemical potential. The functional $F[\rho]$ is universal and independent of the external potential V_{ext} . We can obtain the energy $E[\rho]$ of an individual system if we have the potential associated to the structure and electron density because Hohenberg Kohn theorem gives one to one



mapping of the quantities mentioned. Though we cannot solve the exact $F[\rho]$, but it is hard to approximate because we simplified the unknown from many-variable wave function Ψ to a single three-variable function ρ . To get the minimal energy, what we have to do is searching over all possible density. This is the concept of density-functional method for determining the ground-state density and ground-state energy for any system.

2.3 Kohn-Sham method

Kohn and Sham in 1965 developed a method to deal with the kinetic-energy functional $T[\rho]$ which is less accurate but more practical. The method assumed a non-interacting frame and introduced orbitals. In non-interacting system, electrons do not have repulsion between each other. The Hamiltonian is simplified to

$$H_s = T_s + V_{eff} \quad (2.3.1)$$

Considered orbitals wave function sets, the kinetic energy functional $T[\rho]$ can be represented as

$$T[\rho] = \sum_i^M n_i \langle \phi_i | -\frac{1}{2} \nabla^2 | \phi_i \rangle \quad (2.3.2)$$

and the electron density is

$$\rho(\mathbf{r}) = \sum_i^M n_i \sum_s |\phi_i(\mathbf{r}, s)|^2 \quad (2.3.3)$$

where M could be infinite for any interacting system and n_i is the natural orbital occupation number that $0 \leq n_i \leq 1$. In Kohn-Sham method, the above formulas are simpler, namely

$$T_s[\rho] = \sum_i^N \langle \phi_i | -\frac{1}{2} \nabla^2 | \phi_i \rangle \quad (2.3.4)$$



and

$$\rho(\mathbf{r}) = \sum_i^N \sum_s |\phi_i(\mathbf{r}, s)|^2 \quad (2.3.5)$$

which are fully occupied case of (2.3.2) and (2.3.3) with their occupation number $n_i = 1$ for N orbitals and $n_i = 0$ for the rest.

To define effective potential V_{eff} , we assume the ground states solved from the non-interacting frame and the exact Hamiltonian are the same and compare the chemical potentials. The energy of non-interacting frame is

$$E_s[\rho] = T_s[\rho] + \int \rho(\mathbf{r}) V_{eff}(\mathbf{r}) d\mathbf{r} \quad (2.3.6)$$

and the universal term $F[\rho]$ in (2.1.10) can be expressed conveniently to

$$F[\rho] = T_s[\rho] + E_H[\rho] + E_{xc}[\rho] \quad (2.3.7)$$

where the second term is Hartree functional which is electron-electron repulsion energy have the form

$$E_H[\rho] = \frac{1}{2} \iint \frac{\rho(\mathbf{r})\rho(\mathbf{r}')}{|\mathbf{r}-\mathbf{r}'|} d\mathbf{r} d\mathbf{r}' \quad (2.3.8)$$

and the third term is called exchange-correlation energy; it contains the difference between T and T_s , but the exact form is unknown.

$$E_{xc}[\rho] = T[\rho] + V_{ee}[\rho] - T_s[\rho] - E_H[\rho] \quad (2.3.9)$$

The Euler equation for non-interaction frame becomes

$$\mu_s = V_{eff}(\mathbf{r}) + \frac{\delta T_s[\rho]}{\delta \rho(\mathbf{r})}$$



(2.3.10)

Compare (2.2.6) and (2.3.10) and suppose $\rho_s(\mathbf{r}) = \rho(\mathbf{r})$, we have

$$\mu_s - \mu = V_{eff}(\mathbf{r}) - \left[V_{ext}(\mathbf{r}) + \frac{\delta E_H[\rho]}{\delta \rho(\mathbf{r})} + \frac{\delta E_{xc}[\rho]}{\delta \rho(\mathbf{r})} \right] = \text{const.} \quad (2.3.11)$$

and we can define the KS effective potential as

$$V_{eff}(\mathbf{r}) = V_{ext}(\mathbf{r}) + \int \frac{\rho(\mathbf{r}')}{|\mathbf{r}-\mathbf{r}'|} d\mathbf{r}' + V_{xc}(\mathbf{r}) + \text{const.} \quad (2.3.12)$$

The Kohn-Sham method is an iteration process as follows. For a given effective potential V_{eff} , we can obtain $\rho_s(\mathbf{r}) = \rho(\mathbf{r})$ without solving (2.3.10). Instead, we solve the simplified non-interacting Schrödinger equations which are the N one-electron equations

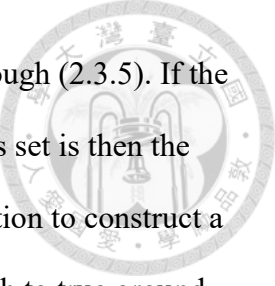
$$\hat{h}(\mathbf{r})\phi_i(\mathbf{r}) = \left[-\frac{1}{2}\nabla^2 + V_{eff}(\mathbf{r}) \right] \phi_i(\mathbf{r}) = \varepsilon_i \phi_i(\mathbf{r}) \quad (2.3.13)$$

which is called Kohn-Sham equation.

For non-interacting fermion systems, the wave function is antisymmetric. We can assume a simple form of single Slater determinant composed by the orbitals solved from (2.3.13) which is antisymmetric and satisfies (2.1.7) and (2.3.5)

$$\Psi = \frac{1}{\sqrt{N!}} \begin{vmatrix} \phi_1(\mathbf{r}_1) & \phi_1(\mathbf{r}_2) & \dots & \phi_1(\mathbf{r}_N) \\ \phi_2(\mathbf{r}_1) & \phi_2(\mathbf{r}_2) & \dots & \phi_2(\mathbf{r}_N) \\ \vdots & \vdots & \ddots & \vdots \\ \phi_N(\mathbf{r}_1) & \phi_N(\mathbf{r}_2) & \dots & \phi_N(\mathbf{r}_N) \end{vmatrix} \quad (2.3.14)$$

To get $\rho_s(\mathbf{r}) = \rho(\mathbf{r})$, the iteration starts from guessing a trial density $\rho_s(\mathbf{r})$ constructing the effective potential (2.3.12), and then solve the Kohn-Sham equation



(2.3.13) to get new orbitals set $\{\phi_i(\mathbf{r})\}$ and the associated $\rho(\mathbf{r})$ through (2.3.5). If the trial density and the new density are the same, this density and orbitals set is then the self-consistent solution. If they do not match, back to the start of iteration to construct a new effective potential and do the process again until it is close enough to true ground state density. Once we have the result, we can obtain the total energy from summing the energy in (2.3.13) and substitute into (2.1.10) together with (2.3.7).

$$\begin{aligned} E[\rho] &= \int \rho(\mathbf{r}) V_{ext}(\mathbf{r}) d\mathbf{r} + T_s[\rho] + E_H[\rho] + E_{xc}[\rho] \\ &= \sum_i^N \varepsilon_i - \frac{1}{2} \int \frac{\rho(\mathbf{r})\rho(\mathbf{r}')}{|\mathbf{r}-\mathbf{r}'|} d\mathbf{r} d\mathbf{r}' + E_{xc}[\rho] - \int V_{xc}(\mathbf{r})\rho(\mathbf{r}) d\mathbf{r} \end{aligned} \quad (2.3.15)$$

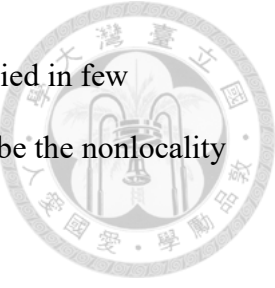
In general, the total energy is not the sum of the orbital energies.

Kohn-Sham DFT has an additional degree of freedom for electron-spin since the effective potential $V_{eff}(\mathbf{r})$ is only spatial without information of spin. For each eigenvalue ε_i , there are two independent solutions sharing the same spatial part. The solutions are doubly degenerate and can be written as

$$\phi_i(\mathbf{r}, s) = \phi_{i\alpha}(\mathbf{r})\alpha(s) + \phi_{i\beta}(\mathbf{r})\beta(s) \quad (2.3.16)$$

so the wave functions satisfy density in (2.3.5). In spin-polarized case, the starting of the original iteration becomes guessing both spin-up and spin-down trial density.

Kohn-Sham method successfully makes DFT practically calculable. It approximates the N-electron system in non-interacting frame and simplifies the Hamiltonian to N one-electron effective Hamiltonians with single Slater determinant solution. The unknown is reduced from $F[\rho]$ to $E_{xc}[\rho]$. The most important improvement is that KS method provides an easy iteration process to get the ground



state quantities and thus KS-DFT has been widely developed and applied in few decades. However, due to the lack of accurate XC functional to describe the nonlocality of XC holes, KS-DFT has some qualitative failures [7][35-37].

2.4 Thermally-Assisted-Occupation density functional theory

For the real N-electron system, the real ground state electron density can be represented for an interacting global external potential in terms of the natural orbitals $\{\chi_i(\mathbf{r})\}$ and natural orbital occupation numbers $\{n_i\}$,

$$\rho_{FCI}(\mathbf{r}) = \sum_{i=1}^{\infty} n_i |\chi_i(\mathbf{r})|^2 \quad (2.4.1)$$

where $\{n_i\}$ follows conditions,

$$\sum_{i=1}^{\infty} n_i = N, \quad 0 \leq n_i \leq 1 \quad (2.4.2)$$

Comparing to the real density, the density in KS-DFT only has its orbitals fully occupied or unoccupied. Although we can obtain nature orbitals occupation numbers by the full configuration interaction (FCI) method, the computational cost is exponentially growing and thus unrealistic.

In 2012, Chai proposed a new method to correct errors in KS-DFT named thermal-assisted-occupation density functional theory (TAO-DFT) [8]. TAO-DFT assumed a non-interacting thermal ensemble external potential representable electron density at a fictitious temperature $\theta \equiv k_B T_{el}$ (where k_B is the Boltzmann constant, T_{el} is the temperature measured in absolute temperature). The density is set to be composed by infinite orbital sets with fractional occupation numbers to approach the real density which can correspondingly expressed as

$$\rho(\mathbf{r}) = \sum_{i=1}^{\infty} f_i |\psi_i(\mathbf{r})|^2 \quad (2.4.3)$$

where f_i is Fermi-Dirac distribution

$$f_i = \{1 + \exp[(\epsilon_i - \mu)/\theta]\}^{-1} \quad (2.4.4)$$



which follows the conditions

$$\sum_{i=1}^{\infty} f_i = N, \quad 0 \leq f_i \leq 1 \quad (2.4.5)$$

where μ is the chemical potential chosen to conserve the number of electrons N .

From section 2.3, the universal functional can be expressed as (2.3.7). Since TAO-DFT has an additional degree of freedom θ , we have to make $F[\rho]$ a θ related functional, start from (2.3.7),

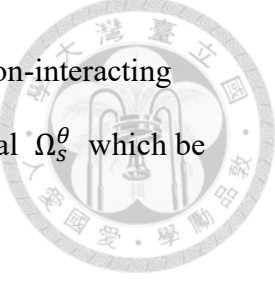
$$\begin{aligned} F[\rho] &= T_s[\rho] + E_H[\rho] + E_{XC}[\rho] \\ &= A_s^\theta[\rho] + E_H[\rho] + (T[\rho] + V_{ee}[\rho] - A_s^\theta[\rho] - E_H[\rho]) \\ &= A_s^\theta[\rho] + E_H[\rho] + (T[\rho] + V_{ee}[\rho] - T_s[\rho] - E_H[\rho]) + (T_s[\rho] - A_s^\theta[\rho]) \\ &= A_s^\theta[\rho] + E_H[\rho] + E_{XC}[\rho] + E_\theta[\rho] \end{aligned} \quad (2.4.6)$$

where $A_s^\theta[\rho]$ is the non-interacting kinetic free energy at temperature θ , and

$$E_\theta[\rho] \equiv T_s[\rho] - A_s^\theta[\rho] = A_s^{\theta=0}[\rho] - A_s^\theta[\rho] \quad (2.4.7)$$

This new universal functional will reduce to the universal functional (2.3.7) in KS-DFT at $\theta = 0$ because the orbitals under fermi energy are fully occupied according to Fermi-Dirac distribution. Minimizing $E[\rho]$ with respect to $\rho(\mathbf{r})$ yields the Euler equation

$$\frac{\delta E[\rho]}{\delta \rho(\mathbf{r})} = \mu = \frac{\delta A_s^\theta[\rho]}{\delta \rho(\mathbf{r})} + v_{ext}(\mathbf{r}) + \int \frac{\rho(\mathbf{r}')}{|\mathbf{r}-\mathbf{r}'|} d\mathbf{r}' + \frac{\delta E_{XC}[\rho]}{\delta \rho(\mathbf{r})} + \frac{\delta E_\theta[\rho]}{\delta \rho(\mathbf{r})} \quad (2.4.8)$$



where μ is the chemical potential. Based on Mermin's theorems, a non-interacting system at temperature θ will have minimum grand-canonical potential Ω_s^θ which be written as

$$\Omega_s^\theta[\rho_s] = A_s^\theta[\rho_s] + \int \rho_s(\mathbf{r})[V_s(\mathbf{r}) - \mu_s] d\mathbf{r} \quad (2.4.9)$$

where μ_s is the chemical potential of the reference system. Minimizing Ω_s^θ yields the Euler equation

$$\mu_s = \frac{\delta A_s^\theta[\rho]}{\delta \rho(\mathbf{r})} + V_s(\mathbf{r}) \quad (2.4.10)$$

Same as (2.3.11), if the both the fictitious density and the real density have the same $\rho_s(\mathbf{r}) = \rho(\mathbf{r})$, we can choose $V_s(\mathbf{r})$ as

$$V_s(\mathbf{r}) = V_{ext}(\mathbf{r}) + \int \frac{\rho(\mathbf{r}')}{|\mathbf{r}-\mathbf{r}'|} d\mathbf{r}' + \frac{\delta E_{XC}[\rho]}{\delta \rho(\mathbf{r})} + \frac{\delta E_\theta[\rho]}{\delta \rho(\mathbf{r})} \quad (2.4.11)$$

This new potential can replace the effective potential $V_{eff}(\mathbf{r})$ in (2.3.13). To obtain a ground-state density using TAO-DFT, the iterating process is similar to one of KS-DFT.

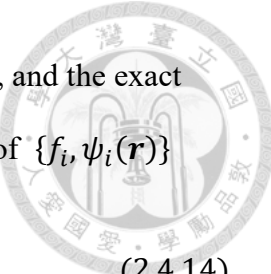
(i) choose a trial $\rho_0(\mathbf{r})$ in (2.4.3) and construct $V_s(\mathbf{r})$ using (2.4.11); (ii) solve Schrödinger equation

$$\left\{ -\frac{1}{2} \nabla^2 + V_s(\mathbf{r}) \right\} \psi_i(\mathbf{r}) = \epsilon_i \psi_i(\mathbf{r}) \quad (2.4.12)$$

to get orbital energy $\{\epsilon_i\}$ and non-interacting electron orbital set $\{\psi_i(\mathbf{r})\}$; (iii) use $\{\epsilon_i\}$ combining with the Fermi-Dirac distribution (2.4.4) and total number (2.4.5)

$$\sum_{i=1}^{\infty} \{1 + \exp[(\epsilon_i - \mu)/\theta]\}^{-1} = N \quad (2.4.13)$$

to find the chemical potential μ ; (iv) determine $\{f_i\}$ in (2.4.4) and new electron density



in (2.4.3). Keep iterating until this procedure reaches the convergence, and the exact non-interacting kinetic free energy $A_s^\theta[\rho]$ can be expressed in terms of $\{f_i, \psi_i(\mathbf{r})\}$

$$A_s^\theta[\{f_i, \psi_i\}] = T_s^\theta[\{f_i, \psi_i\}] - \frac{\theta}{k_B} S_s^\theta[\{f_i\}] \quad (2.4.14)$$

where $T_s^\theta[\{f_i, \psi_i\}]$ is the sum of the kinetic energy

$$\begin{aligned} T_s^\theta[\{f_i, \psi_i\}] &= -\frac{1}{2} \sum_{i=1}^{\infty} f_i \int \psi_i^*(\mathbf{r}) \nabla^2 \psi_i(\mathbf{r}) d\mathbf{r} \\ &= \sum_{i=1}^{\infty} f_i \epsilon_i - \int \rho(\mathbf{r}) V_s(\mathbf{r}) d\mathbf{r} \end{aligned} \quad (2.4.15)$$

and the entropy functional reads

$$S_s^\theta[\{f_i\}] = -k_B \sum_{i=1}^{\infty} [f_i \ln(f_i) + (1-f_i) \ln(1-f_i)] \quad (2.4.16)$$

When the fictitious temperature θ is zero, TAO-DFT reduces to KS-DFT. The term $\frac{\theta}{k_B} S_s^\theta[\{f_i\}]$ do not include information of wave function and is thus believed to describe the nonlocal static correlation where the original KS-DFT is unable to describe properly. Without this term, the degeneracy makes KS-DFT difficult to reach the global minimum dealing with the multi-reference systems. Due to the capability of including static correlation and reasonable efficiency, TAO-DFT is a promising tool to deal with large multi-reference system which high-level ab initio methods are stopped by the exponential computational cost.

2.5 Computational Details

All the calculations are operated under quantum chemistry software Q-chem 4.3 [27][28]. From the length 3 to 8, the results are calculated by spin-restricted and spin-



unrestricted B3LYP with the basis set 6-31G*. The singlet-triplet energy gap (ST gap) is defined as

$$E_{ST} = E_T - E_S \quad (2.21)$$

To compare to the reference, we obtained the energy difference between unrestricted triplet (UT) state, restricted triplet (RT) state, unrestricted singlet (US) state and restricted singlet (RS) state. The original ST gap becomes

$$E_{RT-RS} = E_{RT} - E_{RS}$$

$$E_{RT-US} = E_{RT} - E_{US}$$

$$E_{UT-RS} = E_{UT} - E_{RS}$$

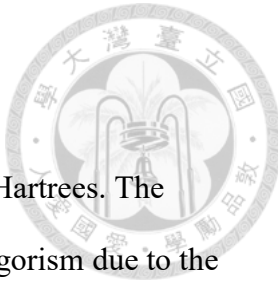
$$E_{UT-U} = E_{UT} - E_{US} \quad (2.22)$$

The results of KS-DFT usually truncate to local minimum, we have to use different initial geometry of go through process with different conditions. The geometries of molecules are built in IQmol 2.13, optimized using universal force field, symmetrized in C2v point group. Each molecule we have only one geometry, but the processes are designed in at least 25 kinds of combination of different conditions. In Qchem, there are several kinds of initial guesses of self-consistent field such as reading from previous calculation, mixing 30% of HOMO and LUMO, core Hamiltonian, generalized Wolfsberg-Helmholtz, basis set projection; also, different SCF algorithms.

For the length 3 to 20, the calculations are based on TAO-LDA and TAO-B3LYP. The fictitious temperature θ for TAO-LDA is set to be 7 mHartrees suggested by the founder where the orbital occupation perform similarly as the natural orbitals [8]. And so is the reason choosing θ set to be 17.4 mHartrees [26]. The basis set of two methods

is 6-31G* and the spin is unrestricted.

For the longer length, the fictitious temperature θ remains 7 mHartrees. The length calculated by the basis set 6-31G* is up to 45 limited by the algorism due to the excessive virtual orbital, but can be up to 75 if the basis set is 6-31G. In convenient, basing on previous experience of TAO calculations, one geometry and one optimizing iteration process could be enough to obtain global minimum.





Chapter 3

Results

The details of the computational results are given in Table 3.1. Figure 3.1 shows the ST gaps of fused acene-azulenes as a function of their length, calculated using both spin-unrestricted and spin-restricted B3LYP as well as the result obtained from spin-unrestricted TAO-B3LYP with its theta 17.4 mhartree. The unrestricted singlet and unrestricted triplet (UT-US) gaps reduce to almost zero rapidly due to the strong correlated effect. The difference between UT-US gaps and restricted triplet (RT)-UT gaps, namely RT-UT gaps basically remain the same as the length increase. However, the difference between UT-US gaps and UT-RS gaps oscillate unexpectedly due to unphysical symmetry-breaking effects. The reference [12] of triplet ground state from the previous study must be related to the UT-RS gaps without the non-monotonic decreasing part. By contrast, the ST gaps calculated using TAO-B3LYP decrease monotonically with increasing of the length.

Table 3.1: The unrestricted singlet (US), unrestricted triplet (UT), restricted singlet (RS) and restricted triplet (RT) state energy of fused-azulene-acene calculated by B3LYP/6-31G* are given in Hartrees. The four kind of singlet-triplet energy gaps are in kcal/mol.

	US	UT	RS	RT	ST gaps					Ref [12]
					UT-US	UT-RS	RT-US	RT-RS		
3	-539.45	-539.43	-539.45	-539.43	12.46	12.46	14.83	14.83	12.45	
4	-693.08	-693.08	-693.08	-693.08	0.08	-2.85	2.85	-0.08	-2.77	
5	-846.72	-846.72	-846.71	-846.72	-0.02	-8.65	3.01	-5.61	-8.53	
6	-1000.36	-1000.36	-1000.34	-1000.36	-0.08	-10.55	3.14	-7.34	-10.61	
7	-1154.00	-1154.00	-1153.98	-1153.99	-0.10	-10.86	3.23	-7.54		
8	-1307.63	-1307.63	-1307.62	-1307.63	-0.10	-10.53	3.30	-7.14		

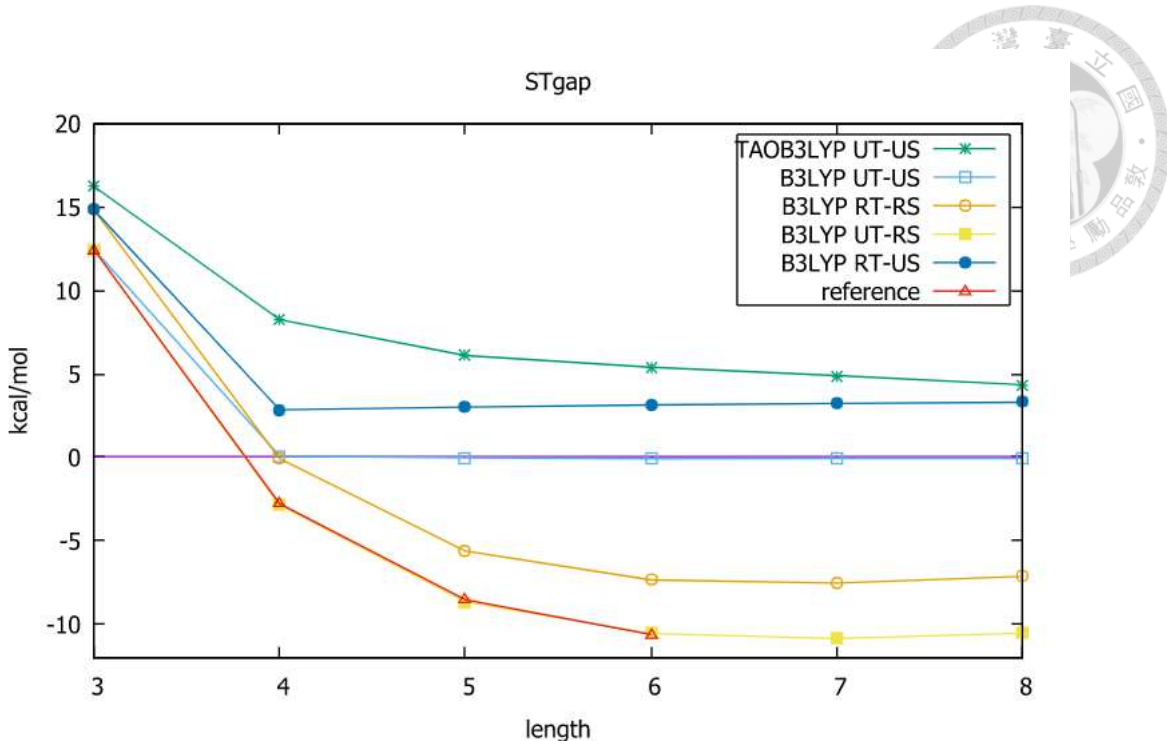


Figure 3.1: Four kinds of singlet-triplet energy gaps of fused-azulene-acene, calculated by B3LYP and TAO-B3LYP ($\theta = 17.4$ mHartree)/6-31G* and reference data [12].

Figure 3.2 shows the ST gaps of n-acenes (GNR[1,n]) and fused azulene-acenes calculated using TAO-LDA and TAO-B3LYP in comparison. The exact values of each line are given in Table 3.2, Table 3.3, Table 3.4 and Table 3.5 respectively. In short length, the boundary defect greatly affects the original acenes, reducing the ST gaps. Though all of the results perform monotonically decreasing, TAO-B3LYP calculations seem to converge faster than the results of TAO-LDA. As the length increase, the ST gaps of fused azulene-acenes and acenes should be less different since the effect of the boundary defect becoming less relevant.

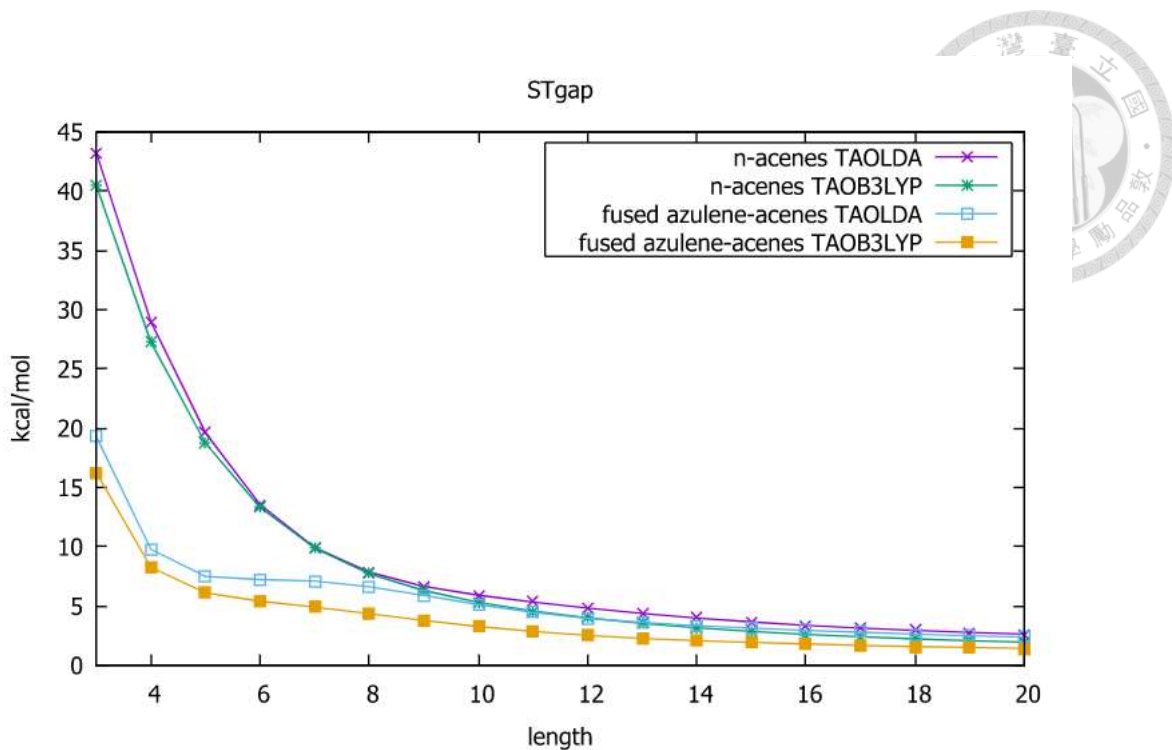


Figure 3.2: Singlet-triplet energy gap of acenes and fused azulene-acenes calculated by TAO-LDA ($\theta = 7$ mHartree)/6-31G* and TAO-B3LYP ($\theta = 17.4$ mHartree)/6-31G*.

Table 3.2: The unrestricted singlet (US) and unrestricted triplet (UT) energy of fused-azulene-acene calculated by TAO-LDA ($\theta = 7$ mHartree)/6-31G* are given in Hartrees. The ST gaps are given in kcal/mol.

	US	UT	ST gap
3	-534.49	-534.46	19.28
4	-686.73	-686.72	9.78
5	-838.97	-838.96	7.49
6	-991.22	-991.21	7.23
7	-1143.46	-1143.45	7.11
8	-1295.70	-1295.69	6.63
9	-1447.94	-1447.94	5.89
10	-1600.19	-1600.18	5.11
11	-1752.43	-1752.42	4.46
12	-1904.67	-1904.66	3.96
13	-2056.91	-2056.90	3.61
14	-2209.15	-2209.15	3.34
15	-2361.39	-2361.39	3.13
16	-2513.63	-2513.63	2.94
17	-2665.88	-2665.87	2.78
18	-2818.12	-2818.11	2.62



19	-2970.36	-2970.36	2.49
20	-3122.60	-3122.60	2.37

Table 3.3: The unrestricted singlet (US) and unrestricted triplet (UT) energy of fused-azulene-acene calculated by TAO-B3LYP ($\theta = 17.4$ mHartree)/6-31G* are given in Hartrees. The ST gaps are given in kcal/mol. The restricted singlet (RS) state energy and the energy difference between RS and US (RS-US) are also listed in Hartrees in comparison.

	US	UT	ST gap	RS	RS-US
3	-539.40	-539.37	16.23	-539.40	-6.62E-05
4	-693.02	-693.01	8.26	-693.02	-9.29E-04
5	-846.64	-846.63	6.10	-846.64	-8.08E-04
6	-1000.27	-1000.26	5.40	-1000.27	-1.53E-03
7	-1153.89	-1153.88	4.90	-1153.89	-1.41E-03
8	-1307.52	-1307.51	4.35	-1307.52	-1.79E-03
9	-1461.14	-1461.13	3.78	-1461.14	-1.80E-03
10	-1614.76	-1614.76	3.26	-1614.76	-2.00E-03
11	-1768.38	-1768.38	2.84	-1768.38	-2.55E-03
12	-1922.01	-1922.00	2.51	-1922.01	-1.50E-03
13	-2075.63	-2075.63	2.26	-2075.63	-2.81E-03
14	-2229.25	-2229.25	2.07	-2229.25	-6.50E-03
15	-2382.88	-2382.87	1.92	-2382.88	-1.17E-03
16	-2536.50	-2536.50	1.79	-2536.50	-1.14E-03
17	-2690.12	-2690.12	1.67	-2690.12	-1.12E-02
18	-2843.75	-2843.74	1.57	-2843.75	-1.03E-02
19	-2997.37	-2997.37	1.49	-2997.37	-1.31E-02
20	-3150.99	-3150.99	1.41	-3150.99	-1.51E-02

Table 3.4: The unrestricted singlet (US) and unrestricted triplet (UT) energy of linear acenes calculated by TAO-LDA ($\theta = 7$ mHartree)/6-31G* are given in Hartrees. The ST gaps are given in kcal/mol.

	US	UT	ST gap
3	-534.56	-534.49	43.22
4	-686.80	-686.76	29.01



5	-839.04	-839.01	19.60
6	-991.28	-991.26	13.55
7	-1143.52	-1143.51	9.91
8	-1295.76	-1295.75	7.84
9	-1448.01	-1448.00	6.66
10	-1600.25	-1600.24	5.90
11	-1752.49	-1752.48	5.32
12	-1904.73	-1904.72	4.82
13	-2056.97	-2056.97	4.37
14	-2209.21	-2209.21	3.98
15	-2361.46	-2361.45	3.65
16	-2513.70	-2513.69	3.37
17	-2665.94	-2665.93	3.14
18	-2818.18	-2818.18	2.94
19	-2970.42	-2970.42	2.77
20	-3122.66	-3122.66	2.62

Table 3.5: The unrestricted singlet (US) and unrestricted triplet (UT) energy of linear acenes calculated by TAO-B3LYP ($\theta = 17.4$ mHartree)/6-31G* are given in Hartrees. The ST gaps are given in kcal/mol.

	US	UT	ST gap
3	-539.47	-539.41	40.44
4	-693.09	-693.05	27.27
5	-846.71	-846.68	18.74
6	-1000.34	-1000.31	13.31
7	-1153.96	-1153.94	9.89
8	-1307.58	-1307.57	7.73
9	-1461.20	-1461.19	6.30
10	-1614.83	-1614.82	5.31
11	-1768.45	-1768.44	4.57
12	-1922.07	-1922.07	3.99
13	-2075.70	-2075.69	3.53
14	-2229.32	-2229.31	3.16
15	-2382.94	-2382.94	2.85
16	-2536.57	-2536.56	2.60
17	-2690.19	-2690.18	2.39



18	-2843.81	-2843.81	2.22
19	-2997.43	-2997.43	2.07
20	-3151.06	-3151.05	1.94

To compare the result to acenes, we expand the system to n being 46 (see Table 3.6) and 75 (see Table 3.7) calculated by TAO-LDA ($\theta = 7$ mHartree) with the basis set 6-31G* and 6-31G since the 6-31G* calculation cannot truncate correctly. From Figure 3.3 we see that the results of this two basis have only little difference, thus we choose the 6-31G result comparing with acenes in Figure 3.4. The difference between fused azulene-acenes and acenes does decrease as the length increase.

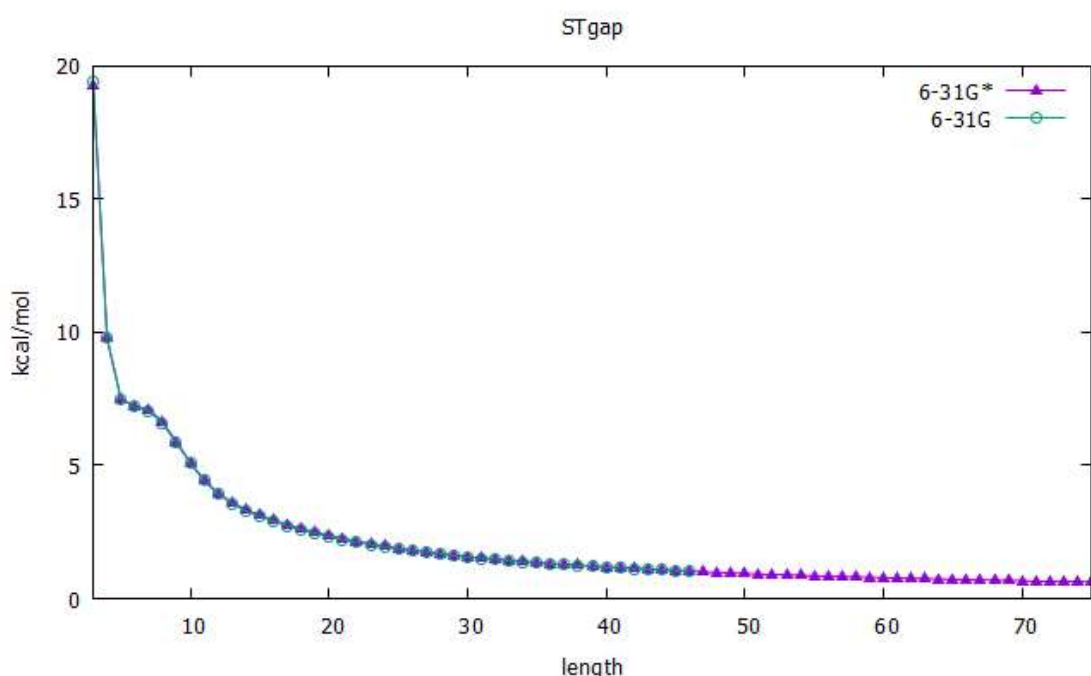


Figure 3.3: Singlet-triplet energy gap of fused azulene-acenes for n from 3 to 46 calculated by TAO-LDA ($\theta = 7$ mHartree)/6-31G* and for n from 3 to 75 calculated by TAO-LDA ($\theta = 7$ mHartree)/6-31G.

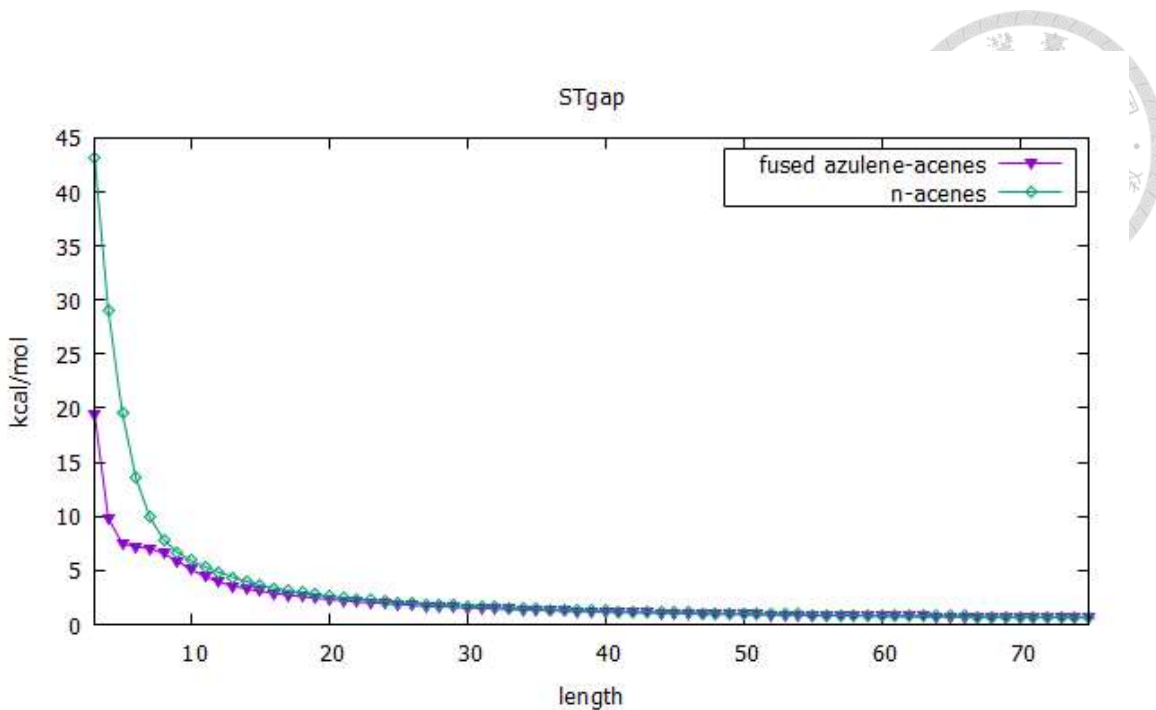


Figure 3.4: Singlet-triplet energy gap for the longer acenes [13] and fused azulene-acenes calculated by TAO-LDA ($\theta = 7$ mHartree)/6-31G.

Table 3.6: The unrestricted singlet (US) and unrestricted triplet (UT) energy of fused-azulene-acene and acenes calculated by TAO-LDA ($\theta = 7$ mHartree)/6-31G* are given in Hartrees. The ST gaps of both fused-azulene-acene and acene are given in kcal/mol.

	fused-azulene-acene			acene
	US	UT	ST gap	ST gap
3	-534.49	-534.46	19.28	43.22
4	-686.73	-686.72	9.78	29.01
5	-838.97	-838.96	7.49	19.60
6	-991.22	-991.21	7.23	13.55
7	-1143.46	-1143.45	7.11	9.91
8	-1295.70	-1295.69	6.63	7.85
9	-1447.94	-1447.94	5.89	6.66
10	-1600.19	-1600.18	5.11	5.91
11	-1752.43	-1752.42	4.46	5.32
12	-1904.67	-1904.66	3.96	4.82
13	-2056.91	-2056.90	3.61	4.38
14	-2209.15	-2209.15	3.34	3.98
15	-2361.39	-2361.39	3.13	3.65
16	-2513.63	-2513.63	2.94	3.37
17	-2665.88	-2665.87	2.78	3.14
18	-2818.12	-2818.11	2.62	2.94
19	-2970.36	-2970.36	2.49	2.77



20	-3122.60	-3122.60	2.36	2.62
21	-3274.84	-3274.84	2.25	2.49
22	-3427.08	-3427.08	2.15	2.37
23	-3579.33	-3579.32	2.06	2.25
24	-3731.57	-3731.56	1.97	2.15
25	-3883.81	-3883.81	1.89	2.06
26	-4036.05	-4036.05	1.82	1.98
27	-4188.29	-4188.29	1.76	1.90
28	-4340.53	-4340.53	1.69	1.83
29	-4492.77	-4492.77	1.64	1.76
30	-4645.02	-4645.01	1.58	1.70
31	-4797.26	-4797.25	1.53	1.64
32	-4949.50	-4949.50	1.49	1.59
33	-5101.74	-5101.74	1.44	1.54
34	-5253.98	-5253.98	1.40	1.49
35	-5406.22	-5406.22	1.36	1.45
36	-5558.46	-5558.46	1.32	1.40
37	-5710.71	-5710.70	1.29	1.36
38	-5862.95	-5862.95	1.26	1.33
39	-6015.19	-6015.19	1.22	1.29
40	-6167.43	-6167.43	1.19	1.26
41	-6319.67	-6319.67	1.17	1.23
42	-6471.91	-6471.91	1.14	1.20
43	-6624.16	-6624.15	1.11	1.17
44	-6776.40	-6776.40	1.09	1.14
45	-6928.64	-6928.64	1.06	1.11
46	-7080.88	-7080.88	1.04	1.09

Biradical character or even polyyradical character of molecules can be judged quantitatively by natural orbital occupation numbers (NOONs) [23]. The NOONs can offer the evidence of polyyradical character of molecules, since the NOONs are either 0 (fully unoccupied) or 2 (fully occupied) in the single-reference system. NOONs between 2 and 0 may be interpreted as fractionally occupied electrons. In Figure 3.6, we plot the active orbital occupation numbers for the lowest singlet state of fused azulene-acene as a function of the ribbon length, calculated using spin-restricted TAO-LDA($\theta =$

7 mHartree)/6-31G. Here, the highest occupied molecular orbital (HOMO) is the $(N/2)$ th orbital, and the lowest unoccupied molecular orbital (LUMO) is the $(N/2 + 1)$ th orbital, with the N being the number of the electrons in fused azulene-acene. As shown, the number of fractionally occupied orbitals increasing with the increase of ribbon length, supporting the fused azulene-acenes have polyyradical character similar to acenes.

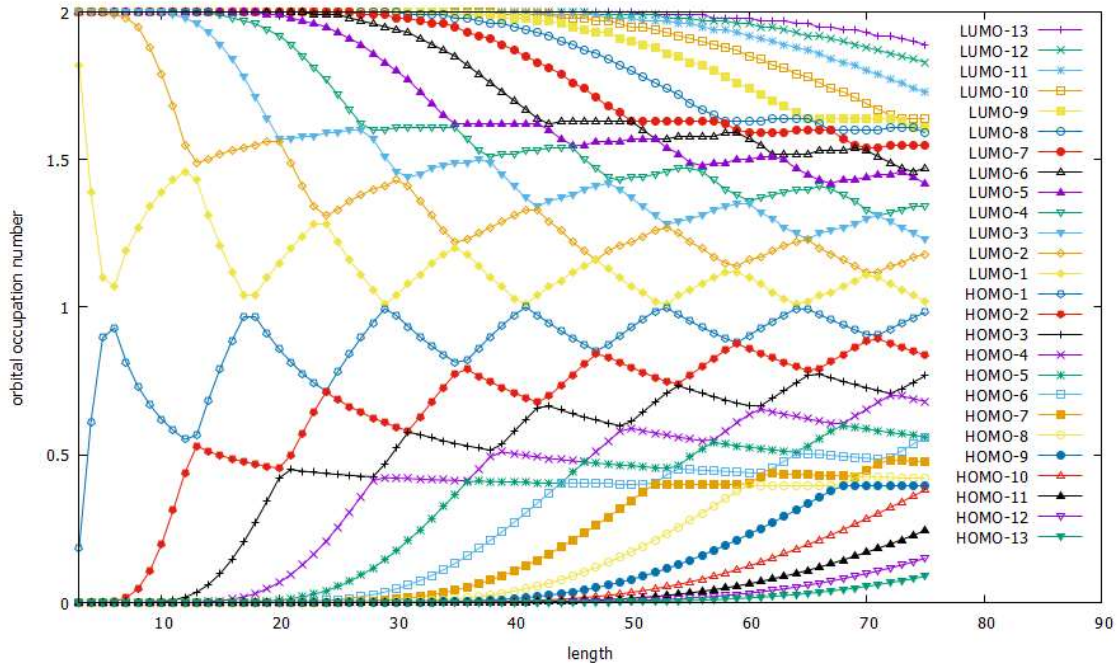
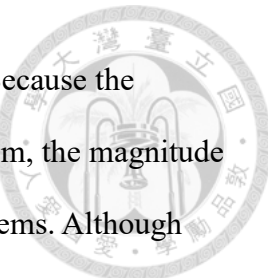


Figure 3.5: Active orbital occupation numbers (HOMO-13, ..., HOMO-1, HOMO, LUMO, LUMO-1, ..., and LUMO-13) as a function of the fused azulene-acene length calculated using spin-restricted TAO-LDA ($\theta = 7$ mHartree)/6-31G.

A quantitative criterion to measure the static correlation is the symmetrized von Neumann entropy [17][24].

$$S = -\frac{1}{2} \sum_i [f_i \ln(f_i) + (1 - f_i) \ln(1 - f_i)] \quad (3.1)$$

which is the symmetrized form of the von Neumann entropy, $S = -\sum_i f_i \ln(f_i)$ [25]. The von Neumann entropy, a scalar extracted from the occupation number array, is a



wave function based criterion to measure the static correlation error. Because the symmetrized von Neumann entropy are zero for single-reference system, the magnitude can be referred to as an index to judge the static correlation in the systems. Although symmetrized von Neumann entropy lost some detailed information in the process of extraction, the one-dimensional number character also provide a simple way to measure the degree of polyyradical or severeness of static correlation. As Figure 3.6 shown, the slope of the symmetrized von Neumann entropy of fused azulene-acenes and acenes are the same, but the difference between two line is a constant for the long ribbon length. According to active orbital occupation numbers of the lowest singlet state of the spin-restricted fused azulene-acene (Figure 3.6), the patterns of the fractional occupation of the two are similar, though the occupation numbers of fused azulene-acene turns to fractional earlier than that of acenes [13]. This may support the translation of the symmetrized von Neumann entropy.

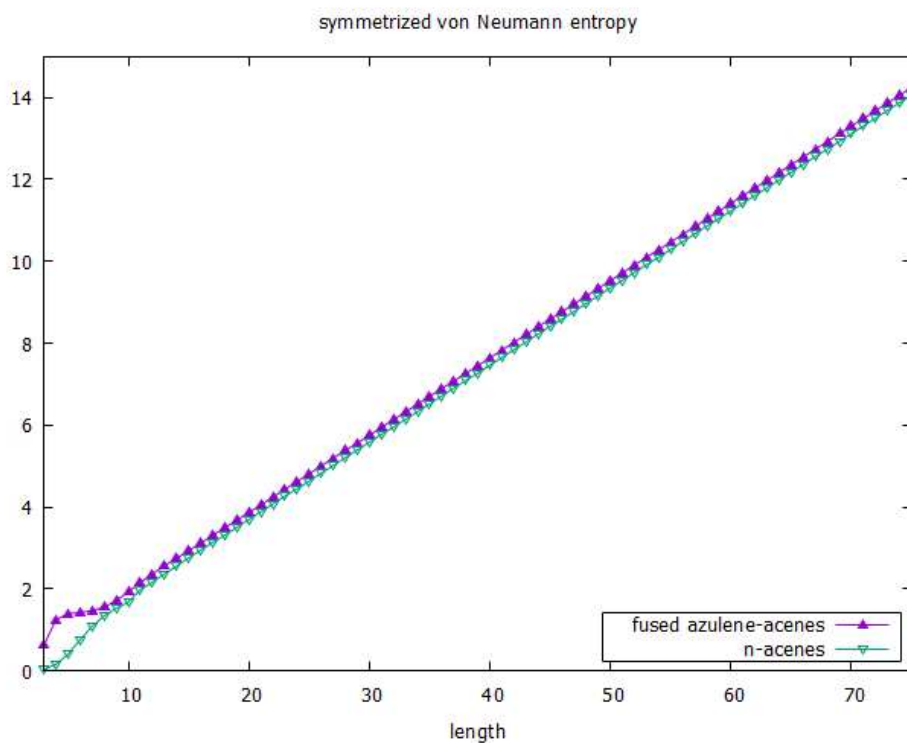


Figure 3.6: Symmetrized von Neumann entropy for the lowest singlet state of fused azulene-acenes and acenes calculated using spin-restricted TAO-LDA ($\theta = 7$ mHartree)/6-31G.

Table 3.7: The unrestricted singlet (US) and the unrestricted triplet (UT) energy of fused azulene-acenes calculated by TAO-LDA ($\theta = 7$ mHartree)/6-31G are given in Hartrees. The ST gaps of fused azulene-acene, acenes [13] and Δ are given in kcal/mol where Δ is the difference between ST gaps of fused azulene-acene and acenes. The dipole moment of US and UT and the singlet-triplet dipole moment gap are given in debyes. The symmetrized von Neumann entropy of both fused azulene-acene and acenes [13] are given.

	fused-azulene-acene			acene		fused-azulene-acene			acene	
	US	UT	ST gap	ST gap	Δ	$\mu(\text{US})$	$\mu(\text{UT})$	$\mu(\text{UT-US})$	svNe	svNe
3	-534.36	-534.33	19.43	43.22	23.79	2.63	-0.04	-2.66	0.62	0.03
4	-686.56	-686.55	9.80	29.01	19.21	2.98	0.80	-2.17	1.24	0.15
5	-838.77	-838.75	7.48	19.60	12.12	2.80	1.89	-0.90	1.39	0.40
6	-990.97	-990.96	7.19	13.55	6.36	2.65	2.89	0.24	1.42	0.75
7	-1143.18	-1143.17	7.05	9.91	2.86	2.62	3.56	0.94	1.46	1.08
8	-1295.38	-1295.37	6.57	7.85	1.28	2.70	3.89	1.19	1.55	1.34
9	-1447.59	-1447.58	5.84	6.66	0.82	2.85	4.02	1.16	1.71	1.52
10	-1599.79	-1599.78	5.08	5.91	0.83	3.06	4.08	1.02	1.92	1.67
11	-1751.99	-1751.99	4.42	5.32	0.90	3.27	4.13	0.85	2.15	1.98
12	-1904.20	-1904.19	3.93	4.82	0.89	3.48	4.20	0.72	2.36	2.16
13	-2056.40	-2056.39	3.57	4.38	0.81	3.67	4.30	0.63	2.56	2.36
14	-2208.60	-2208.60	3.30	3.98	0.68	3.85	4.42	0.57	2.74	2.55
15	-2360.81	-2360.80	3.08	3.65	0.57	4.01	4.55	0.54	2.93	2.75
16	-2513.01	-2513.01	2.90	3.37	0.47	4.17	4.69	0.51	3.11	2.94
17	-2665.21	-2665.21	2.73	3.14	0.41	4.34	4.83	0.49	3.30	3.13
18	-2817.42	-2817.41	2.58	2.94	0.36	4.50	4.97	0.48	3.49	3.31
19	-2969.62	-2969.62	2.45	2.77	0.32	4.66	5.12	0.46	3.67	3.50
20	-3121.83	-3121.82	2.32	2.62	0.30	4.83	5.26	0.43	3.86	3.69
21	-3274.03	-3274.03	2.21	2.49	0.28	4.99	5.40	0.41	4.05	3.88
22	-3426.23	-3426.23	2.11	2.37	0.26	5.15	5.55	0.40	4.24	4.07
23	-3578.44	-3578.43	2.02	2.25	0.23	5.32	5.69	0.38	4.43	4.26
24	-3730.64	-3730.64	1.94	2.15	0.21	5.48	5.84	0.36	4.62	4.44
25	-3882.84	-3882.84	1.86	2.06	0.20	5.64	5.99	0.35	4.81	4.63
26	-4035.05	-4035.04	1.79	1.98	0.19	5.80	6.14	0.34	5.00	4.82
27	-4187.25	-4187.25	1.72	1.90	0.18	5.95	6.28	0.33	5.19	5.01
28	-4339.46	-4339.45	1.66	1.83	0.17	6.12	6.43	0.31	5.38	5.20
29	-4491.66	-4491.66	1.61	1.76	0.15	6.28	6.58	0.30	5.56	5.39
30	-4643.86	-4643.86	1.55	1.70	0.15	6.43	6.72	0.30	5.75	5.58
31	-4796.07	-4796.06	1.50	1.64	0.14	6.59	6.87	0.28	5.94	5.77

32	-4948.27	-4948.27	1.46	1.59	0.13	6.74	7.01	0.27	6.13	5.95
33	-5100.47	-5100.47	1.41	1.54	0.13	6.89	7.16	0.27	6.32	6.14
34	-5252.68	-5252.68	1.37	1.49	0.12	7.05	7.31	0.26	6.51	6.33
35	-5404.88	-5404.88	1.33	1.45	0.12	7.21	7.46	0.25	6.70	6.52
36	-5557.08	-5557.08	1.30	1.40	0.10	7.37	7.61	0.23	6.89	6.71
37	-5709.29	-5709.29	1.26	1.36	0.10	7.52	7.75	0.24	7.07	6.90
38	-5861.49	-5861.49	1.23	1.33	0.10	7.67	7.90	0.22	7.26	7.09
39	-6013.70	-6013.69	1.20	1.29	0.09	7.83	8.05	0.22	7.45	7.27
40	-6165.90	-6165.90	1.17	1.26	0.09	7.98	8.19	0.22	7.64	7.46
41	-6318.10	-6318.10	1.14	1.23	0.09	8.13	8.34	0.21	7.83	7.65
42	-6470.31	-6470.30	1.12	1.20	0.08	8.28	8.49	0.21	8.02	7.84
43	-6622.51	-6622.51	1.09	1.17	0.08	8.43	8.64	0.21	8.21	8.03
44	-6774.71	-6774.71	1.07	1.14	0.07	8.57	8.78	0.21	8.40	8.22
45	-6926.92	-6926.92	1.04	1.11	0.07	8.73	8.94	0.21	8.59	8.41
46	-7079.12	-7079.12	1.02	1.09	0.07	8.88	9.07	0.20	8.77	8.59
47	-7231.33	-7231.32	1.00	1.07	0.07	9.02	9.21	0.19	8.96	8.78
48	-7383.53	-7383.53	0.98	1.04	0.06	9.16	9.35	0.18	9.15	8.97
49	-7535.73	-7535.73	0.96	1.02	0.06	9.33	9.49	0.16	9.34	9.16
50	-7687.94	-7687.93	0.94	1.00	0.06	9.48	9.64	0.16	9.53	9.35
51	-7840.14	-7840.14	0.92	0.98	0.06	9.62	9.80	0.17	9.72	9.54
52	-7992.34	-7992.34	0.90	0.96	0.06	9.77	9.93	0.17	9.91	9.73
53	-8144.55	-8144.55	0.89	0.94	0.05	9.91	10.08	0.17	10.10	9.92
54	-8296.75	-8296.75	0.87	0.92	0.05	10.04	10.22	0.18	10.28	10.10
55	-8448.95	-8448.95	0.85	0.91	0.06	10.20	10.37	0.17	10.47	10.29
56	-8601.16	-8601.16	0.84	0.89	0.05	10.34	10.50	0.16	10.66	10.48
57	-8753.36	-8753.36	0.83	0.87	0.04	10.49	10.67	0.17	10.85	10.67
58	-8905.57	-8905.56	0.81	0.86	0.05	10.66	10.81	0.16	11.04	10.86
59	-9057.77	-9057.77	0.80	0.84	0.04	10.82	10.93	0.11	11.23	11.05
60	-9209.97	-9209.97	0.78	0.83	0.05	10.93	11.07	0.14	11.42	11.23
61	-9362.18	-9362.18	0.77	0.82	0.05	11.10	11.22	0.12	11.61	11.42
62	-9514.38	-9514.38	0.76	0.80	0.04	11.23	11.35	0.13	11.79	11.61
63	-9666.58	-9666.58	0.75	0.79	0.04	11.46	11.50	0.04	11.98	11.80
64	-9818.79	-9818.79	0.74	0.78	0.04	11.68	11.65	-0.03	12.17	11.99
65	-9970.99	-9970.99	0.72	0.76	0.04	11.65	11.83	0.18	12.36	12.18
66	-10123.20	-10123.19	0.71	0.75	0.04	11.81	11.93	0.13	12.55	12.37
67	-10275.40	-10275.40	0.70	0.74	0.04	11.93	12.11	0.18	12.74	12.56
68	-10427.60	-10427.60	0.69	0.73	0.04	12.07	12.39	0.32	12.93	12.74
69	-10579.81	-10579.81	0.68	0.72	0.04	12.25	12.49	0.24	13.12	12.93

70	-10732.01	-10732.01	0.67	0.71	0.04	12.37	12.48	0.11	13.31	13.12	
71	-10884.21	-10884.21	0.66	0.70	0.04	12.49	12.61	0.12	13.49	13.31	
72	-11036.42	-11036.42	0.66	0.69	0.03	12.65	12.75	0.10	13.68	13.50	
73	-11188.62	-11188.62	0.65	0.68	0.03	12.83	12.89	0.06	13.87	13.69	
74	-11340.82	-11340.82	0.64	0.67	0.03	12.98	13.05	0.07	14.06	13.88	
75	-11493.03	-11493.03	0.63	0.66	0.03	13.12	13.18	0.06	14.25	14.06	

From Figure 3.7 to Figure 3.10, we show the real-space representation of shortest four lowest singlet states of fused azulene-acene obtained with spin-restricted TAO-LDA since we find a curve crossing behavior in the approach to single occupation with increasing length. The shape of orbitals of HOMO and LUMO exchange at the point where the curve cross. The curve crossing behavior may be an artifact showing the limitation of TAO-LDA (with a system-independent θ) [13]. In addition of mainly localized at the edge of acenes in previous studies [13][17], the orbital of long-chain fused azulene-acene shown in Appendix B have nodes, and the amount of nodes increases with the length periodically.

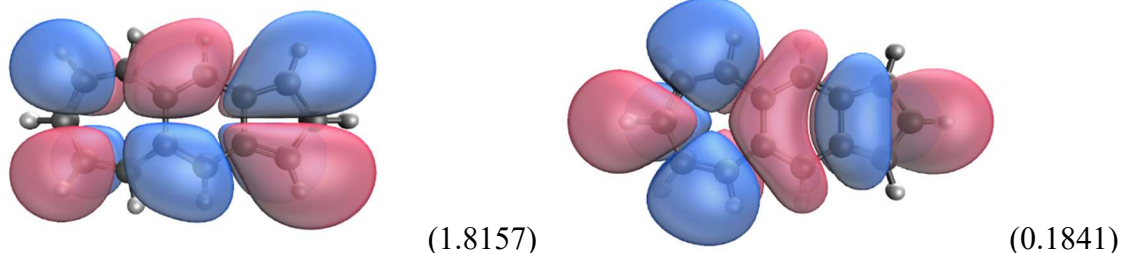


Figure 3.7: Real-space representation of HOMO (left) and LUMO (right) for the singlet state of fused azulene-acene ($n=3$) with their occupation number 1.8157 and 0.1841

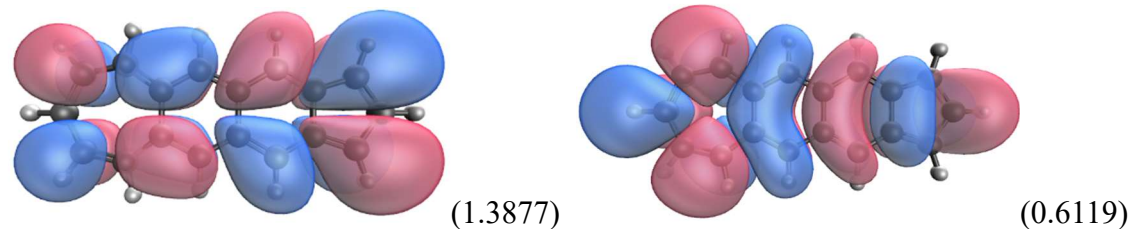


Figure 3.8: Real-space representation of HOMO (left) and LUMO (right) for the singlet state of fused azulene-acene ($n=4$) with their occupation number 1.3877 and 0.6119

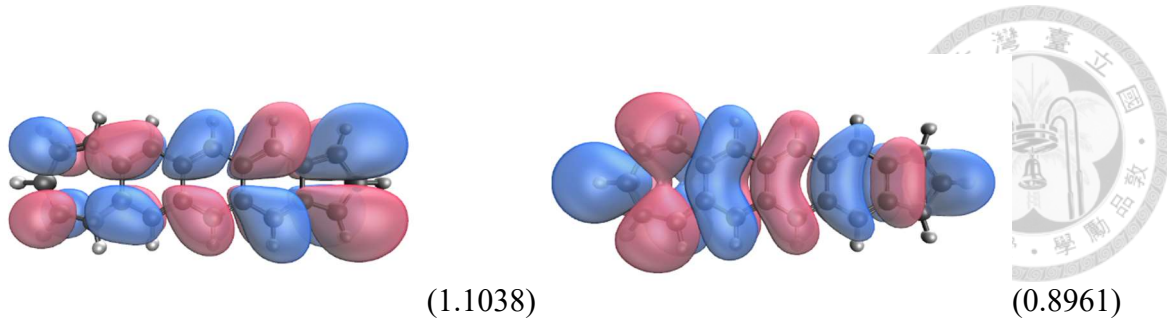


Figure 3.9: Real-space representation of HOMO (left) and LUMO (right) for the singlet state of fused azulene-acene ($n=5$) with their occupation number 1.1038 and 0.8961

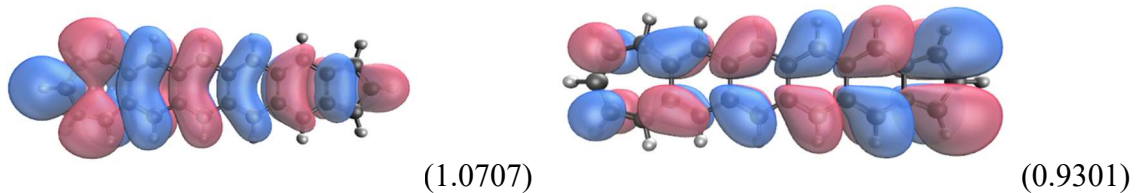


Figure 3.10: Real-space representation of HOMO (left) and LUMO (right) for the singlet state of fused azulene-acene ($n=6$) with their occupation number 1.0707 and 0.9301

Polarity can affect ST gap on the aromatic compound [14]. To study the detail of how the ST gaps are tuned, in Figure 3.7, we show the differences between ST gap of acene and fused azulene-acene and the dipole moment singlet triplet gap. The dipole moment of both unrestricted singlet state and unrestricted triplet state increase monotonically in Table 3.7, though the polarity inverse when n less than 6. In the short length, the two quantities have negative correlation. As the length increase, polarity has less influence in tuning the ST gap, though there is zigzag on the line, which we do not know that it is error during converging or the character of this system. Since we only use one geometry and one iteration process, the failed results may be truncated to local minimum, though other properties perform well or be too small to be realized.

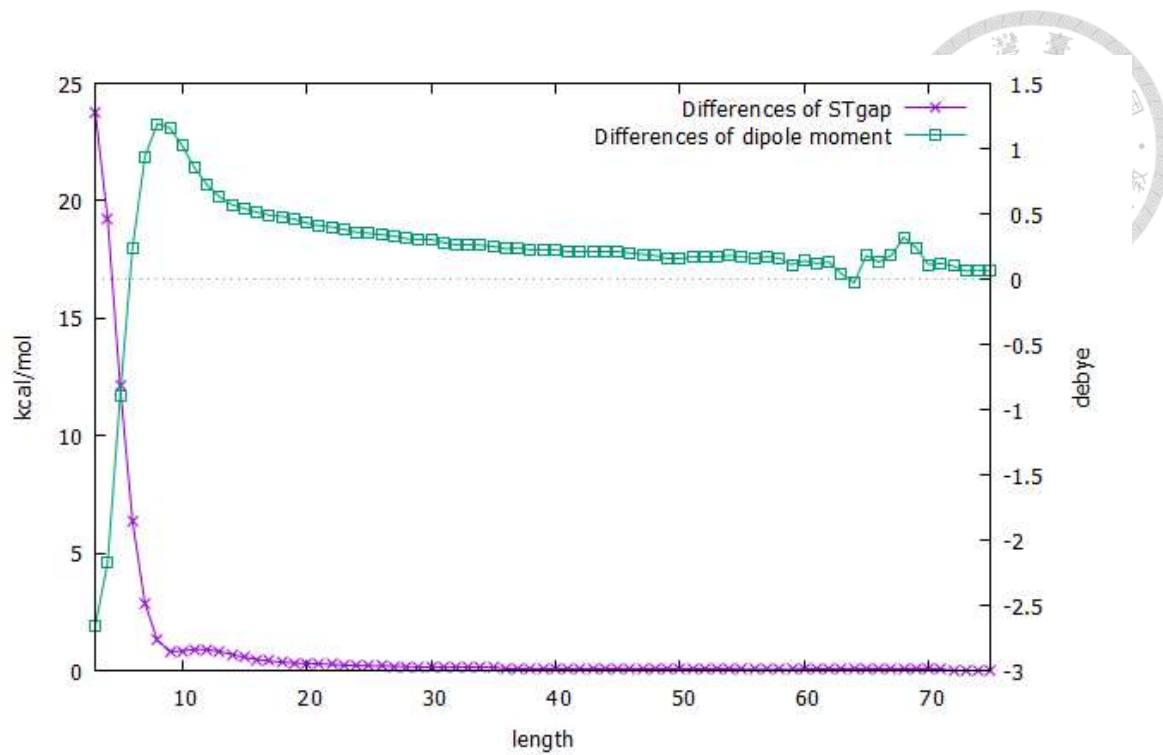


Figure 3.11: Differences between STgap of n-acenes [13] and fused azulene-acene and dipole moment difference between single and triplet state of fused azulene-acene calculating using spin-unrestricted TAO-LDA ($\theta = 7$ mHartree)/6-31G.



Chapter 4

Conclusion

TAO-LDA is a more efficient method and also greatly corrects static correlation error in Kohn-Sham LDA. The expensive calculation cost makes TAO-LDA easily applied on larger molecules. In this study, it is used to explore electronic properties of linear isomers of polyacenes which have its two ends replaced by 7 and 5 carbon rings. We predict that the fused azulene-acene should be singlet ground state instead of triplet ground state, and also reproduce the KS calculations to show that the results varies under different conditions with different physical meaning. Fractional orbital occupation numbers and nonzero symmetrized von Neumann entropy can be the evidence of polyyradical properties of this acene-like system. Fused azulene-acene do has similar orbital occupation structure to acene. Besides, the results calculated by TAO-LDA provides a way to tune the ST gap by adding dipole moment. However, the affect is limited for large molecules.

In future, this system can be expanded to 2D finite size of other combination of 5 and 7 rings, though it is hard to deal with lots of combinations on the edge. Also it could be hard to compare with its zigzag graphene nanoribbons isomers because the structure and polarity. Other way to create polarity flipping could be dosing different atoms in acene to tune ST gaps for wider applications.



Chapter 5

Reference

- [1] Donald A. Neamen, Semiconductor Physics and Devices: basic principles, Fourth Edition (McGraw-Hill, New York, 2012).
- [2] K. S. Novoselov, A.K. Geim. Two-dimensional gas of massless Dirac fermions in graphene. *Nature* 438 (2005), 197-200.
- [3] G.P. Tang, J.C. Zhou, Z.H. Zhang, X.Q. Deng, Z.Q. Fan. A theoretical investigation on the possible improvement of spin-filter effects by an electric field for a zigzag graphene nanoribbon with a line defect. *Carbon* 60 (2013), 94-101.
- [4] S. R. Yost, J. Lee, M. W. Wilson, T. Wu, D. P. McMahon, R. R. Parkhurst, N. J. Thompson, D. N. Congreve, A. Rao, K. Johnson, M. Y. Sfeir, M. G. Bawendi, T. M. Swager, R. H. Friend, M. A. Baldo and T. V. Voorhis. A transferable model for singlet-fission kinetics. *Nature Chemistry* 6 (2014), 492-497.
- [5] M. B. Smith and J. Michl, Singlet Fission. *Chem. Rev.* 110 (2010), 6891–6936.
- [6] M. Bendikov, H. M. Duong, K. Starkey, K. Houk, E. A. Carter and F. Wudl, J. Oligoacenes: Theoretical Prediction of Open-Shell Singlet Diradical Ground States. *America Chemical Society* 126 (2004), 7416–7417.
- [7] A. J. Cohen, P. Mori-Sánchez, and W. Yang. Insights into current limitations of density functional theory. *Science* 321 (2008), 792-794.



- [8] Jeng-Da Chai. Density functional theory with fractional orbital occupations. *The Journal of Chemical Physics* 136, 154104 (2012).
- [9] G.P. Tang, J.C. Zhou, Z.H. Zhang, X.Q. Deng, Z.Q. Fan. A theoretical investigation on the possible improvement of spin-filter effects by an electric field for a zigzag graphene nanoribbon with a line defect. *Carbon* 60 (2013), 94-101.
- [10] Hachmann J., Dorando J. J., Aviles M., Chan G. K. L. The radical character of the acenes: a density matrix renormalization group study. *Journal of Chemical Physics* 127, 134309 (2007).
- [11] K. Pelzer, L. Greenman, G. Gidofalvi, D. A. Mazziotti. Analytical gradients of variational reduced-density-matrix and wavefunction-based methods from an overlap-reweighted semidefinite program. *Journal of Chemical Physics* 115, 5632 (2011).
- [12] Madhumita Rano, Sumanta K. Ghosh and Debasree Ghosh. In the quest for a stable triplet state in small polycyclic aromatic hydrocarbons: an in silico tool for rational design and prediction. *Chemical Science* 10 (2019), 9270-9276.
- [13] C. S. Wu and J. D. Chai. Electronic properties of zigzag graphene nanoribbons studies by TAO-DFT. *Journal of Chemical Theory and Computation* 11 (2015), 2003-2011.
- [14] H. Ottosson, K. Kilså, K. Chajara, M. C. Piqueras, R. Crespo, H. Kato and D. Muthas. Scope and limitations of Braid's theory on triplet state aromaticity: application to the tuning of singlet-triplet energy gaps in fulvenes. *Chemistry – A European Journal* 13 (2007), 6998-7005.
- [15] N. C. Braid. Quantum organic photochemistry. II. resonance and aromaticity in the

lowest $\pi\pi^*$ state of cyclic hydrocarbons. *Journal of the American Chemical Society* 94 (1972), 4941-4948.



[16] H. Möllerstedt, M. C. Piqueras, R. Crespo, and H. Ottosson. Fulvenes, fulvalenes, and azulene: are they aromatic chameleons? *Journal of the American Chemical Society* 126 (2004), 13938-13939.

[17] P. Rivero, C.A. Jiménez-Hoyos, G. E. Scuseria. Entanglement and polyyradical character of polycyclic aromatic hydrocarbons predicted by projected Hartree-Fock theory. *The Journal of Physical Chemistry B* 117 (2013), 12750-12758.

[18] A. Hirohata and K. Takanashi. Future perspectives for spintronic devices. *Journal of Physics D: Applied Physics* 47 (2014), 193001.

[19] S. Thomas, S. Ramasesha, K. Hallberg and D. Garcia. Fused azulene as possible organic multiferroics. *Physical Review B* 86 (2012), 180403.

[20] Z. Qu, S. Zhang, C. Liu, and J.-P. Malrieu. Communication: a dramatic transition from nonferromagnet to ferromagnet in finite fused-azulene chain. *The Journal of Chemical Physics* 134 (2011), 021101.

[21] P. Hohenberg and W. Kohn. Inhomogeneous electron gas. *Physical Review* 136 (1964), B864-B871.

[22] W. Kohn and L. J. Sham. Self-consistent equations including exchange and correlation effects. *Physical Review* 140 (1965), A1133-A1138.

[23] D. Döhnert and J. Koutecký. Occupation numbers of natural orbitals as a criterion for biradical character. Different kinds of biradicals. *Journal of the American Chemical Society* 102:6 (1980), 1789-1795.



- [24] K. Samanta, C. A. Jiménez-Hoyos, and G. E. Scuseria. Exploring copper oxide cores using the projected Hartree-Fock method. *Journal of Chemical Theory and Computation* 8 (2012), 4944-4949.
- [25] U. R. Fogueri, S. Kozuch, A. Karton, J. M. L. Martin. A simple DFT-based diagnostic for nondynamical correlation. *Theoretical Chemistry Accounts* 132 (2013), 1921.
- [26] Jeng-Da Chai. Role of exact exchange in thermally-assisted-occupation density functional theory: a proposal of new hybrid schemes. *The Journal of Chemical Physics* 146 (2017), 044102.
- [27] Y. Shao, Z. Gan, E. Epifanovsky, A. T. B. Gilbert, M. Wormit, J. Kussmann, A. W. Lange, A. Behn, J. Deng, X. Feng, D. Ghosh, M. Goldey, P. R. Horn, L. D. Jacobson, I. Kaliman, R. Z. Khaliullin, T. Kuś, A. Landau, J. Liu, E. I. Proynov, Y. M. Rhee, R. M. Richard, M. A. Rohrdanz, R. P. Steele, E. J. Sundstrom, H. L. Woodcock III, P. M. Zimmerman, D. Zuev, B. Albrecht, E. Alguire, B. Austin, G. J. O. Beran, Y. A. Bernard, E. Berquist, K. Brandhorst, K. B. Bravaya, S. T. Brown, D. Casanova, C. M. Chang, Y. Q. Chen, S. H. Chien, K. D. Closser, D. L. Crittenden, M. Diedenhofen, R. A. DiStasio Jr., H. Do, A. D. Dutoi, R. G. Edgar, S. Fatehi, L. Fusti-Molnar, A. Ghysels, A. Golubeva-Zadorozhnaya, J. Gomes, M. W.D. Hanson-Heine, P. H.P. Harbach, A. W. Hauser, E. G. Hohenstein, Z. C. Holden, Thomas-C. Jagau, H. Ji, B. Kaduk, K. Khistyayev, J. Kim, J. Kim, R. A. King, P. Klunzinger, D. Kosenkov, T. Kowalczyk, C. M. Krauter, K. U. Lao, A. D. Laurent, K. V. Lawler, S. V. Levchenko, C. Y. Lin, F. Liu, E. Livshits, R. C. Lochan, A. Luenser, P. Manohar, S. F. Manzer, S. P. Mao, N. Mardirossian, A. V. Marenich, S. A. Maurer, N. J. Mayhall, E. Neuscamman, C. M. Oana, R. Olivares-Amaya, D. P. O'Neill, J. A. Parkhill, T. M. Perrine, R. Peverati, A.



Prociuk, D. R. Rehn, E. Rosta, N. J. Russ, S. M. Sharada, S. Sharma, D. W. Small, A. Sodt, T. Stein, D. Stück, Y. C. Su, A. J.W. Thom, T. Tsuchimochi, V. Vanovschi, L. Vogt, O. Vydrov, T. Wang, M. A. Watson, J. Wenzel, A. White, C. F. Williams, J. Yang, S. Yeganeh, S. R. Yost, Z. Q. You, I. Y. Zhang, X. Zhang, Y. Zhao, B. R. Brooks, G. K.L. Chan, D. M. Chipman, C. J. Cramer, W. A. Goddard III, M. S. Gordon, W. J. Hehre, A. Klamt, H. F. Schaefer III, M. W. Schmidt, C. D. Sherrill, D. G. Truhlar, A. Warshel, X. Xu, A. Aspuru-Guzik, R. Baer, A. T. Bell, N. A. Besley, J. D. Chai, A. Dreuw, B. D. Dunietz, T. R. Furlani, S. R. Gwaltney, C. P. Hsu, Y. Jung, J. Kong, D. S. Lambrecht, W. Z. Liang, C. Ochsenfeld, V. A. Rassolov, L. V. Slipchenko, J. E. Subotnik, T. Van Voorhis, J. M. Herbert, A. I. Krylov, P. M.W. Gill & Martin Head-Gordon. Advances in molecular quantum chemistry contained in the Q-Chem 4 program package. *Molecular Physics* 113:2 (2015), 184-215

[28] A. I. Krylov, P. M.W. Gill. Q-chem: an engine for innovation. *Computational Molecular Science* 3:317 (2013).

[29] Y. Zhang, Y. W. Tan, H. L. Stormer, P. Kim. Experimental observation of the quantum Hall effect and Berry's phase in graphene. *Nature* 438 (2005), 201-204.

[30] M. Y. Han, B. Özyilmaz, Y. Zhang, and P. Kim. Energy band-gap of engineering of graphene nanoribbons. *Physical Review Letters* 98 (2007), 206805.

[31] S. Kim, J. Ihm, H. J. Choi, Y. W. Son. Origin of anomalous electronic structures of epitaxial graphene on silicon carbide. *Physical Review Letters* 100 (2008), 176802.

[32] Y. W. Son, M. L.Cohen, S. G. Louie. Energy gaps in graphene nanoribbons. *Physical Review Letters* 97 (2006), 216803.

[33] K. Pelzer, L. Greenman, G. Gidofalvi, D. A. Mazziotti. Strong correlation in acene



sheets from the active-space variational two-electron reduced density matrix method effects of symmetry and size. *The Journal of Physical Chemistry A* 115 (2011), 5632-5640.

[34] C. Y. Lin, K. Hui, J. H. Chung, J. D. Chai. Self-consistent determination of the fictitious temperature in thermally-assisted-occupation density functional theory. *The Royal Society of Chemistry Advances* 7 (2017), 50496-50507.

[35] T. Bally and G. N. Sastry. Incorrect dissociation behavior of radical ions in density functional calculations. *The Journal of Physical Chemistry A* 101 (1997), 7923.

[36] A. Dreuw, J. L. Weisman, and M. Head-Gordon. Long-range charge-transfer excited states in time-dependent density functional theory require non-local exchange. *The Journal of Chemical Physics* 119 (2003), 2943.

[37] J. F. Dobson, K. McLennan, A. Rubio, J. Wang, T. Gould, H. M. Le, B. P. Dinte. Prediction of dispersion forces: Is there a problem? *Australian Journal of Chemistry* 54 (2001).



Appendix A: Active orbital occupation numbers for the lowest singlet states of fused azulene-acene

Table A: Active orbital occupation numbers (HOMO-13, ..., HOMO-1, LUMO-1, ..., LUMO-13) for the lowest singlet states of fused azulene-acene, calculated by spin-restricted TAO-LDA ($\theta = 7$ mHartree), using the 6-31G basis set.

	f_{H-13}	f_{H-12}	f_{H-11}	f_{H-10}	f_{H-9}	f_{H-8}	f_{H-7}	f_{H-6}	f_{H-5}	f_{H-4}	f_{H-3}	f_{H-2}	f_{H-1}		
3	2.0000	2.0000	2.0000	2.0000	2.0000	2.0000	2.0000	2.0000	2.0000	2.0000	2.0000	1.9999	1.8156		
4	2.0000	2.0000	2.0000	2.0000	2.0000	2.0000	2.0000	2.0000	2.0000	2.0000	1.9999	1.9998	1.3873		
5	2.0000	2.0000	2.0000	2.0000	2.0000	2.0000	2.0000	2.0000	2.0000	2.0000	1.9998	1.9991	1.1029		
6	2.0000	2.0000	2.0000	2.0000	2.0000	2.0000	2.0000	2.0000	2.0000	2.0000	1.9998	1.9949	1.0703		
7	2.0000	2.0000	2.0000	2.0000	2.0000	2.0000	2.0000	2.0000	2.0000	2.0000	1.9999	1.9998	1.9810	1.1877	
8	2.0000	2.0000	2.0000	2.0000	2.0000	2.0000	2.0000	2.0000	2.0000	2.0000	1.9998	1.9995	1.9474	1.2739	
9	2.0000	2.0000	2.0000	2.0000	2.0000	2.0000	2.0000	2.0000	2.0000	2.0000	1.9998	1.9982	1.8848	1.3403	
10	2.0000	2.0000	2.0000	2.0000	2.0000	2.0000	2.0000	2.0000	2.0000	2.0000	1.9999	1.9998	1.9952	1.7914	1.3923
11	2.0000	2.0000	2.0000	2.0000	2.0000	2.0000	2.0000	2.0000	2.0000	2.0000	1.9998	1.9996	1.9887	1.6757	1.4319
12	2.0000	2.0000	2.0000	2.0000	2.0000	2.0000	2.0000	1.9999	1.9998	1.9990	1.9766	1.5498	1.4626		
13	2.0000	2.0000	2.0000	2.0000	2.0000	2.0000	2.0000	1.9998	1.9998	1.9977	1.9568	1.4862	1.4256		
14	2.0000	2.0000	2.0000	2.0000	2.0000	2.0000	2.0000	1.9998	1.9996	1.9952	1.9274	1.5049	1.3101		
15	2.0000	2.0000	2.0000	2.0000	2.0000	2.0000	1.9999	1.9998	1.9992	1.9910	1.8873	1.5200	1.2067		
16	2.0000	2.0000	2.0000	2.0000	2.0000	2.0000	1.9998	1.9998	1.9985	1.9844	1.8365	1.5327	1.1159		
17	2.0000	2.0000	2.0000	2.0000	2.0000	2.0000	1.9998	1.9997	1.9973	1.9745	1.7762	1.5435	1.0371		
18	2.0000	2.0000	2.0000	2.0000	2.0000	1.9999	1.9998	1.9994	1.9952	1.9605	1.7086	1.5528	1.0404		
19	2.0000	2.0000	2.0000	2.0000	2.0000	1.9998	1.9998	1.9989	1.9922	1.9418	1.6362	1.5608	1.1017		
20	2.0000	2.0000	2.0000	2.0000	1.9999	1.9998	1.9997	1.9981	1.9877	1.9179	1.5678	1.5615	1.1546		
21	2.0000	2.0000	2.0000	2.0000	1.9999	1.9998	1.9995	1.9970	1.9815	1.8886	1.5740	1.4869	1.2005		
22	2.0000	2.0000	2.0000	2.0000	1.9998	1.9998	1.9991	1.9953	1.9732	1.8539	1.5794	1.4140	1.2403		
23	2.0000	2.0000	2.0000	1.9999	1.9998	1.9997	1.9986	1.9929	1.9624	1.8142	1.5841	1.3442	1.2751		
24	2.0000	2.0000	2.0000	1.9999	1.9998	1.9995	1.9978	1.9896	1.9489	1.7700	1.5884	1.3057	1.2782		
25	2.0000	2.0000	2.0000	1.9998	1.9998	1.9993	1.9968	1.9852	1.9322	1.7223	1.5922	1.3326	1.2164		
26	2.0000	2.0000	1.9999	1.9998	1.9997	1.9989	1.9953	1.9796	1.9124	1.6719	1.5956	1.3564	1.1592		
27	2.0000	2.0000	1.9999	1.9998	1.9996	1.9983	1.9933	1.9724	1.8893	1.6197	1.5987	1.3775	1.1063		
28	2.0000	1.9999	1.9998	1.9998	1.9994	1.9976	1.9907	1.9636	1.8629	1.6015	1.5665	1.3964	1.0577		
29	2.0000	1.9999	1.9998	1.9997	1.9991	1.9966	1.9874	1.9530	1.8335	1.6041	1.5133	1.4133	1.0130		
30	2.0000	1.9999	1.9998	1.9996	1.9986	1.9953	1.9832	1.9403	1.8013	1.6064	1.4606	1.4285	1.0378		
31	1.9999	1.9998	1.9998	1.9994	1.9981	1.9936	1.9781	1.9256	1.7666	1.6086	1.4423	1.4090	1.0771		
32	1.9999	1.9998	1.9997	1.9992	1.9974	1.9915	1.9719	1.9088	1.7297	1.6105	1.4547	1.3590	1.1131		
33	1.9999	1.9998	1.9996	1.9989	1.9965	1.9888	1.9644	1.8897	1.6911	1.6124	1.4660	1.3108	1.1460		
34	1.9998	1.9998	1.9995	1.9984	1.9953	1.9856	1.9557	1.8685	1.6513	1.6140	1.4763	1.2646	1.1761		
35	1.9998	1.9997	1.9993	1.9979	1.9938	1.9816	1.9456	1.8452	1.6156	1.6105	1.4857	1.2206	1.2037		
36	1.9998	1.9996	1.9990	1.9972	1.9920	1.9770	1.9340	1.8200	1.6170	1.5693	1.4943	1.2291	1.1788		
37	1.9998	1.9995	1.9987	1.9964	1.9898	1.9714	1.9208	1.7930	1.6184	1.5279	1.5023	1.2524	1.1393		
38	1.9997	1.9993	1.9983	1.9953	1.9872	1.9650	1.9062	1.7644	1.6196	1.5096	1.4868	1.2738	1.1020		
39	1.9997	1.9991	1.9977	1.9940	1.9841	1.9576	1.8900	1.7344	1.6208	1.5163	1.4462	1.2936	1.0669		
40	1.9995	1.9988	1.9971	1.9924	1.9804	1.9492	1.8722	1.7031	1.6219	1.5226	1.4062	1.3119	1.0338		
41	1.9994	1.9985	1.9963	1.9906	1.9761	1.9396	1.8530	1.6710	1.6229	1.5283	1.3672	1.3287	1.0059		
42	1.9992	1.9981	1.9953	1.9884	1.9711	1.9290	1.8324	1.6381	1.6239	1.5337	1.3444	1.3293	1.0367		
43	1.9990	1.9976	1.9941	1.9858	1.9654	1.9172	1.8104	1.6248	1.6047	1.5387	1.3589	1.2925	1.0656		
44	1.9987	1.9969	1.9928	1.9828	1.9590	1.9043	1.7872	1.6256	1.5710	1.5434	1.3724	1.2571	1.0928		
45	1.9984	1.9962	1.9912	1.9793	1.9518	1.8902	1.7628	1.6264	1.5478	1.5372	1.3849	1.2229	1.1182		
46	1.9979	1.9953	1.9893	1.9753	1.9438	1.8750	1.7376	1.6271	1.5518	1.5036	1.3966	1.1901	1.1420		
47	1.9974	1.9943	1.9871	1.9708	1.9349	1.8586	1.7114	1.6278	1.5556	1.4702	1.4075	1.1644	1.1587		
48	1.9968	1.9930	1.9846	1.9658	1.9251	1.8412	1.6845	1.6285	1.5592	1.4371	1.4177	1.1854	1.1285		

	49	1.9961	1.9916	1.9817	1.9601	1.9144	1.8227	1.6570	1.6291	1.5626	1.4273	1.4046	1.2052	1.0997
50	1.9953	1.9900	1.9784	1.9538	1.9028	1.8033	1.6297	1.6290	1.5657	1.4362	1.3726	1.2237	1.0723	
51	1.9944	1.9881	1.9747	1.9469	1.8904	1.7830	1.6303	1.6007	1.5687	1.4447	1.3414	1.2412	1.0460	
52	1.9932	1.9859	1.9706	1.9392	1.8770	1.7618	1.6308	1.5723	1.5715	1.4526	1.3109	1.2577	1.0210	
53	1.9920	1.9835	1.9661	1.9309	1.8628	1.7399	1.6314	1.5742	1.5437	1.4600	1.2812	1.2732	1.0119	
54	1.9905	1.9807	1.9610	1.9219	1.8477	1.7173	1.6318	1.5767	1.5152	1.4670	1.2878	1.2524	1.0360	
55	1.9889	1.9777	1.9554	1.9121	1.8318	1.6942	1.6323	1.5791	1.4868	1.4737	1.3015	1.2245	1.0588	
56	1.9870	1.9742	1.9493	1.9017	1.8151	1.6706	1.6328	1.5814	1.4799	1.4587	1.3146	1.1974	1.0806	
57	1.9849	1.9705	1.9426	1.8905	1.7977	1.6466	1.6332	1.5835	1.4858	1.4308	1.3269	1.1713	1.1013	
58	1.9825	1.9663	1.9354	1.8786	1.7797	1.6336	1.6223	1.5856	1.4914	1.4033	1.3385	1.1460	1.1210	
59	1.9799	1.9617	1.9276	1.8660	1.7610	1.6340	1.5978	1.5875	1.4967	1.3763	1.3495	1.1397	1.1217	
60	1.9770	1.9567	1.9193	1.8527	1.7417	1.6343	1.5894	1.5732	1.5017	1.3600	1.3497	1.1575	1.0983	
61	1.9738	1.9512	1.9103	1.8388	1.7219	1.6347	1.5911	1.5484	1.5065	1.3699	1.3237	1.1745	1.0757	
62	1.9703	1.9453	1.9007	1.8243	1.7016	1.6350	1.5928	1.5237	1.5110	1.3793	1.2983	1.1906	1.0539	
63	1.9665	1.9390	1.8906	1.8091	1.6809	1.6354	1.5944	1.5153	1.4991	1.3882	1.2734	1.2060	1.0330	
64	1.9623	1.9321	1.8799	1.7933	1.6599	1.6357	1.5959	1.5195	1.4746	1.3967	1.2491	1.2207	1.0129	
65	1.9577	1.9248	1.8686	1.7771	1.6387	1.6360	1.5974	1.5234	1.4503	1.4047	1.2347	1.2255	1.0158	
66	1.9528	1.9170	1.8568	1.7603	1.6363	1.6172	1.5988	1.5271	1.4262	1.4124	1.2480	1.2025	1.0355	
67	1.9475	1.9087	1.8444	1.7430	1.6365	1.6001	1.5956	1.5306	1.4197	1.4025	1.2607	1.1802	1.0544	
68	1.9419	1.9000	1.8314	1.7254	1.6368	1.6014	1.5738	1.5340	1.4267	1.3790	1.2728	1.1585	1.0726	
69	1.9358	1.8907	1.8180	1.7074	1.6371	1.6026	1.5520	1.5373	1.4334	1.3559	1.2844	1.1374	1.0900	
70	1.9293	1.8809	1.8041	1.6890	1.6373	1.6038	1.5404	1.5302	1.4397	1.3332	1.2955	1.1170	1.1067	
	$f_{L-1} \quad f_{L-2} \quad f_{L-3} \quad f_{L-4} \quad f_{L-5} \quad f_{L-6} \quad f_{L-7} \quad f_{L-8} \quad f_{L-9} \quad f_{L-10} \quad f_{L-11} \quad f_{L-12} \quad f_{L-13}$													
3	0.1842	0.0004	0.0000	0.0000	0.0000	0.0000	0.0000	0.0000	0.0000	0.0000	0.0000	0.0000	0.0000	0.0000
4	0.6124	0.0006	0.0000	0.0000	0.0000	0.0000	0.0000	0.0000	0.0000	0.0000	0.0000	0.0000	0.0000	0.0000
5	0.8970	0.0006	0.0006	0.0000	0.0000	0.0000	0.0000	0.0000	0.0000	0.0000	0.0000	0.0000	0.0000	0.0000
6	0.9305	0.0039	0.0006	0.0000	0.0000	0.0000	0.0000	0.0000	0.0000	0.0000	0.0000	0.0000	0.0000	0.0000
7	0.8151	0.0159	0.0005	0.0001	0.0000	0.0000	0.0000	0.0000	0.0000	0.0000	0.0000	0.0000	0.0000	0.0000
8	0.7323	0.0464	0.0005	0.0003	0.0000	0.0000	0.0000	0.0000	0.0000	0.0000	0.0000	0.0000	0.0000	0.0000
9	0.6698	0.1055	0.0011	0.0005	0.0000	0.0000	0.0000	0.0000	0.0000	0.0000	0.0000	0.0000	0.0000	0.0000
10	0.6208	0.1969	0.0032	0.0005	0.0001	0.0000	0.0000	0.0000	0.0000	0.0000	0.0000	0.0000	0.0000	0.0000
11	0.5829	0.3125	0.0082	0.0006	0.0002	0.0000	0.0000	0.0000	0.0000	0.0000	0.0000	0.0000	0.0000	0.0000
12	0.5532	0.4400	0.0180	0.0006	0.0005	0.0000	0.0000	0.0000	0.0000	0.0000	0.0000	0.0000	0.0000	0.0000
13	0.5669	0.5303	0.0349	0.0014	0.0006	0.0001	0.0000	0.0000	0.0000	0.0000	0.0000	0.0000	0.0000	0.0000
14	0.6858	0.5125	0.0610	0.0030	0.0006	0.0002	0.0000	0.0000	0.0000	0.0000	0.0000	0.0000	0.0000	0.0000
15	0.7929	0.4983	0.0979	0.0060	0.0006	0.0004	0.0000	0.0000	0.0000	0.0000	0.0000	0.0000	0.0000	0.0000
16	0.8873	0.4867	0.1460	0.0111	0.0008	0.0006	0.0001	0.0000	0.0000	0.0000	0.0000	0.0000	0.0000	0.0000
17	0.9694	0.4770	0.2045	0.0189	0.0016	0.0006	0.0001	0.0000	0.0000	0.0000	0.0000	0.0000	0.0000	0.0000
18	0.9689	0.4686	0.2716	0.0305	0.0029	0.0006	0.0003	0.0000	0.0000	0.0000	0.0000	0.0000	0.0000	0.0000
19	0.9100	0.4615	0.3446	0.0466	0.0050	0.0006	0.0005	0.0001	0.0000	0.0000	0.0000	0.0000	0.0000	0.0000
20	0.8590	0.4552	0.4208	0.0678	0.0082	0.0010	0.0006	0.0001	0.0000	0.0000	0.0000	0.0000	0.0000	0.0000
21	0.8148	0.4979	0.4498	0.0945	0.0129	0.0017	0.0006	0.0002	0.0000	0.0000	0.0000	0.0000	0.0000	0.0000
22	0.7763	0.5736	0.4450	0.1270	0.0195	0.0028	0.0006	0.0004	0.0001	0.0000	0.0000	0.0000	0.0000	0.0000
23	0.7427	0.6466	0.4408	0.1649	0.0283	0.0044	0.0007	0.0006	0.0001	0.0000	0.0000	0.0000	0.0000	0.0000
24	0.7158	0.7132	0.4370	0.2078	0.0398	0.0067	0.0011	0.0006	0.0002	0.0000	0.0000	0.0000	0.0000	0.0000
25	0.7807	0.6872	0.4337	0.2550	0.0542	0.0100	0.0018	0.0006	0.0003	0.0001	0.0000	0.0000	0.0000	0.0000
26	0.8410	0.6642	0.4307	0.3055	0.0718	0.0143	0.0027	0.0006	0.0005	0.0001	0.0000	0.0000	0.0000	0.0000
27	0.8967	0.6437	0.4280	0.3585	0.0927	0.0199	0.0041	0.0008	0.0006	0.0002	0.0000	0.0000	0.0000	0.0000
28	0.9479	0.6255	0.4256	0.4130	0.1171	0.0270	0.0059	0.0013	0.0006	0.0003	0.0001	0.0000	0.0000	0.0000
29	0.9948	0.6091	0.4680	0.4234	0.1449	0.0358	0.0082	0.0019	0.0006	0.0004	0.0001	0.0000	0.0000	0.0000
30	0.9722	0.5944	0.5228	0.4214	0.1758	0.0466	0.0113	0.0027	0.0007	0.0006	0.0002	0.0000	0.0000	0.0000
31	0.9347	0.5812	0.5767	0.4195	0.2096	0.0594	0.0152	0.0038	0.0010	0.0006	0.0002	0.0001	0.0000	0.0000
32	0.9005	0.6293	0.5692	0.4178	0.2460	0.0744	0.0201	0.0053	0.0014	0.0006	0.0004	0.0001	0.0000	0.0000
33	0.8690	0.6801	0.5583	0.4163	0.2845	0.0916	0.0261	0.0071	0.0019	0.0006	0.0005	0.0001	0.0000	0.0000
34	0.8403	0.7288	0.5483	0.4148	0.3248	0.1111	0.0333	0.0095	0.0027	0.0008	0.0006	0.0002	0.0001	0.0000
35	0.8138	0.7754	0.5392	0.4135	0.3663	0.1329	0.0418	0.0124	0.0036	0.0011	0.0006	0.0003	0.0001	0.0000
36	0.8196	0.7895	0.5309	0.4123	0.4086	0.1569	0.0517	0.0160	0.0048	0.0015	0.0006	0.0004	0.0001	0.0000
37	0.8614	0.7672	0.5233	0.4514	0.4111	0.1829	0.0632	0.0203	0.0064	0.0020	0.0006	0.0006	0.0002	0.0000
38	0.9009	0.7466	0.5163	0.4942	0.4101	0.2108	0.0762	0.0254	0.0082	0.0026	0.0009	0.0006	0.0003	0.0000
39	0.9381	0.7276	0.5366	0.5098	0.4091	0.2404	0.0908	0.0315	0.0105	0.0035	0.0012	0.0006	0.0004	0.0000
40	0.9730	0.7100	0.5785	0.5038	0.4082	0.2715	0.1071	0.0385	0.0133	0.0045	0.0015	0.0006	0.0005	0.0000

41	1.0028	0.6937	0.6196	0.4983	0.4073	0.3038	0.1250	0.0466	0.0166	0.0058	0.0020	0.0007	0.0006
42	0.9736	0.6786	0.6597	0.4931	0.4065	0.3372	0.1445	0.0557	0.0204	0.0073	0.0026	0.0009	0.0006
43	0.9462	0.6985	0.6646	0.4883	0.4057	0.3713	0.1654	0.0661	0.0250	0.0092	0.0034	0.0012	0.0006
44	0.9205	0.7361	0.6516	0.4838	0.4059	0.4050	0.1878	0.0776	0.0302	0.0114	0.0043	0.0016	0.0006
45	0.8963	0.7724	0.6395	0.4797	0.4409	0.4043	0.2116	0.0903	0.0361	0.0140	0.0054	0.0021	0.0008
46	0.8737	0.8071	0.6282	0.4759	0.4758	0.4038	0.2365	0.1042	0.0429	0.0170	0.0067	0.0026	0.0010
47	0.8524	0.8406	0.6177	0.5107	0.4722	0.4032	0.2625	0.1193	0.0504	0.0206	0.0082	0.0033	0.0013
48	0.8725	0.8323	0.6078	0.5453	0.4688	0.4026	0.2895	0.1357	0.0589	0.0246	0.0101	0.0041	0.0017
49	0.9031	0.8135	0.5985	0.5796	0.4656	0.4020	0.3173	0.1532	0.0683	0.0291	0.0122	0.0050	0.0021
50	0.9323	0.7957	0.6132	0.5899	0.4626	0.4015	0.3457	0.1718	0.0786	0.0343	0.0146	0.0062	0.0026
51	0.9601	0.7790	0.6463	0.5817	0.4597	0.4010	0.3746	0.1914	0.0898	0.0401	0.0174	0.0075	0.0032
52	0.9867	0.7633	0.6786	0.5740	0.4570	0.4039	0.4006	0.2121	0.1020	0.0465	0.0206	0.0090	0.0039
53	0.9972	0.7485	0.7100	0.5668	0.4545	0.4334	0.4001	0.2337	0.1151	0.0537	0.0243	0.0108	0.0048
54	0.9745	0.7406	0.7344	0.5600	0.4631	0.4521	0.3997	0.2560	0.1292	0.0615	0.0283	0.0128	0.0058
55	0.9529	0.7703	0.7212	0.5536	0.4927	0.4498	0.3993	0.2792	0.1442	0.0701	0.0329	0.0152	0.0069
56	0.9323	0.7991	0.7087	0.5475	0.5221	0.4477	0.3989	0.3029	0.1600	0.0794	0.0380	0.0178	0.0082
57	0.9128	0.8269	0.6969	0.5514	0.5418	0.4457	0.3986	0.3272	0.1767	0.0895	0.0435	0.0207	0.0097
58	0.8941	0.8538	0.6857	0.5803	0.5363	0.4437	0.3982	0.3520	0.1943	0.1003	0.0497	0.0240	0.0115
59	0.8797	0.8763	0.6750	0.6089	0.5312	0.4419	0.3979	0.3771	0.2125	0.1119	0.0564	0.0277	0.0134
60	0.9046	0.8594	0.6650	0.6370	0.5263	0.4401	0.4025	0.3976	0.2315	0.1242	0.0637	0.0318	0.0156
61	0.9286	0.8433	0.6646	0.6554	0.5217	0.4385	0.4281	0.3973	0.2512	0.1373	0.0716	0.0362	0.0181
62	0.9518	0.8279	0.6916	0.6463	0.5173	0.4537	0.4369	0.3970	0.2714	0.1511	0.0801	0.0412	0.0208
63	0.9740	0.8133	0.7180	0.6377	0.5131	0.4794	0.4354	0.3967	0.2921	0.1656	0.0892	0.0465	0.0238
64	0.9953	0.7993	0.7438	0.6295	0.5091	0.5050	0.4339	0.3964	0.3133	0.1807	0.0989	0.0524	0.0272
65	0.9936	0.7860	0.7690	0.6217	0.5305	0.5053	0.4326	0.3962	0.3349	0.1965	0.1093	0.0587	0.0308
66	0.9751	0.7935	0.7732	0.6143	0.5558	0.5017	0.4313	0.3959	0.3568	0.2129	0.1203	0.0655	0.0349
67	0.9572	0.8173	0.7611	0.6072	0.5809	0.4983	0.4300	0.3957	0.3790	0.2298	0.1319	0.0728	0.0392
68	0.9401	0.8404	0.7495	0.6057	0.6004	0.4950	0.4288	0.4014	0.3955	0.2473	0.1440	0.0806	0.0440
69	0.9236	0.8628	0.7384	0.6301	0.5940	0.4918	0.4276	0.4240	0.3953	0.2653	0.1568	0.0890	0.0492
70	0.9078	0.8846	0.7278	0.6542	0.5878	0.4888	0.4466	0.4265	0.3950	0.2837	0.1701	0.0978	0.0547
71	0.9057	0.8926	0.7176	0.6779	0.5819	0.4860	0.4693	0.4255	0.3948	0.3025	0.1839	0.1072	0.0607
72	0.9261	0.8780	0.7079	0.7011	0.5763	0.4919	0.4832	0.4245	0.3946	0.3216	0.1983	0.1171	0.0671
73	0.9458	0.8640	0.7239	0.6986	0.5709	0.5145	0.4806	0.4235	0.3945	0.3410	0.2132	0.1275	0.0739
74	0.9650	0.8505	0.7462	0.6897	0.5657	0.5369	0.4780	0.4226	0.3943	0.3607	0.2285	0.1384	0.0811
75	0.9834	0.8376	0.7680	0.6812	0.5608	0.5592	0.4756	0.4216	0.3941	0.3806	0.2442	0.1497	0.0888



Appendix B: Figures of real-space representation of HOMOs and LUMOs for the lowest singlet states of fused azulene-acene calculated using spin-restricted TAO-LDA($\theta = 7$ mHartree) at isovalue = 0.02 eV/Å³

Figure B.1: Real-space representation of HOMO (left) and LUMO (right) for the singlet state of fused azulene-acene ($n=7$) with their occupation number 1.1880 and 0.8147

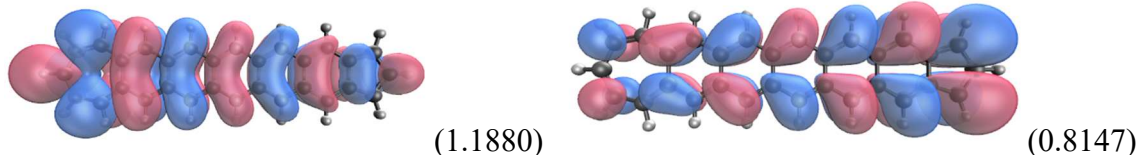


Figure B.2: Real-space representation of HOMO (left) and LUMO (right) for the singlet state of fused azulene-acene ($n=8$) with their occupation number 1.2742 and 0.7320

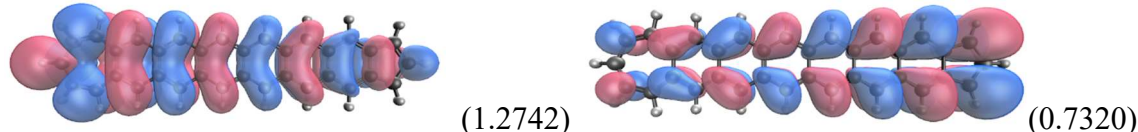


Figure B.3: Real-space representation of HOMO (left) and LUMO (right) for the singlet state of fused azulene-acene ($n=9$) with their occupation number 1.3406 and 0.6694

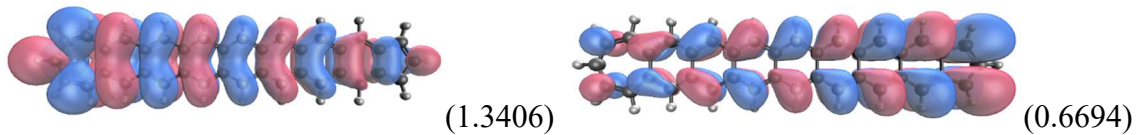


Figure B.4: Real-space representation of HOMO (left) and LUMO (right) for the singlet state of fused azulene-acene ($n=10$) with their occupation number 1.3927 and 0.6203

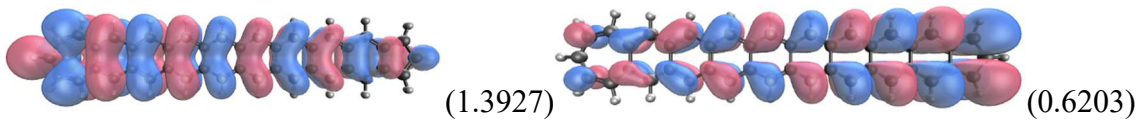


Figure B.5: Real-space representation of HOMO (left) and LUMO (right) for the singlet state of fused azulene-acene ($n=11$) with their occupation number 1.4323 and 0.5825

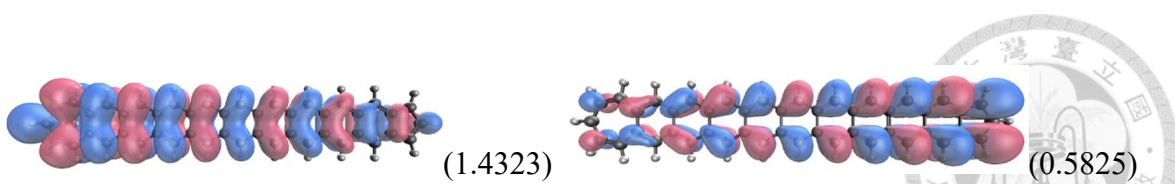


Figure B.6: Real-space representation of HOMO (left) and LUMO (right) for the singlet state of fused azulene-acene ($n=12$) with their occupation number 1.4628 and 0.5529

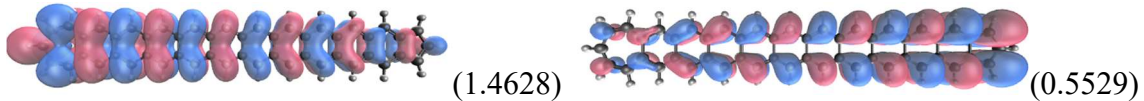


Figure B.7: Real-space representation of HOMO (left) and LUMO (right) for the singlet state of fused azulene-acene ($n=13$) with their occupation number 1.4257 and 0.5668



Figure B.8: Real-space representation of HOMO (left) and LUMO (right) for the singlet state of fused azulene-acene ($n=14$) with their occupation number 1.3102 and 0.6857

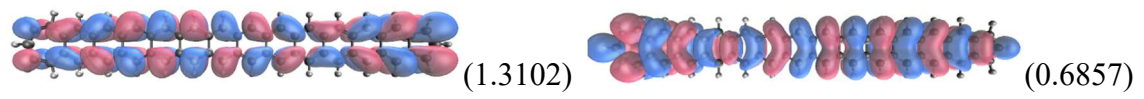


Figure B.9: Real-space representation of HOMO (left) and LUMO (right) for the singlet state of fused azulene-acene ($n=15$) with their occupation number 1.2068 and 0.7927



Figure B.10: Real-space representation of HOMO (left) and LUMO (right) for the singlet state of fused azulene-acene ($n=16$) with their occupation number 1.1160 and 0.8871



Figure B.11: Real-space representation of HOMO (left) and LUMO (right) for the singlet state of fused azulene-acene ($n=17$) with their occupation number 1.0372 and 0.9693

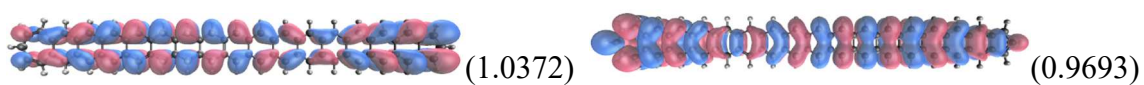


Figure B.12: Real-space representation of HOMO (left) and LUMO (right) for the singlet state of fused azulene-acene ($n=18$) with their occupation number 1.0405 and 0.9688

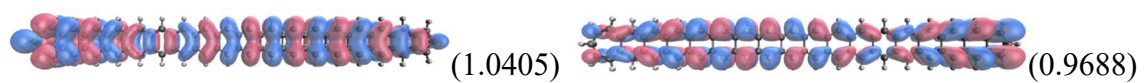


Figure B.13: Real-space representation of HOMO (up) and LUMO (down) for the singlet state of fused azulene-acene ($n=19$) with their occupation number 1.1018 and 0.9099

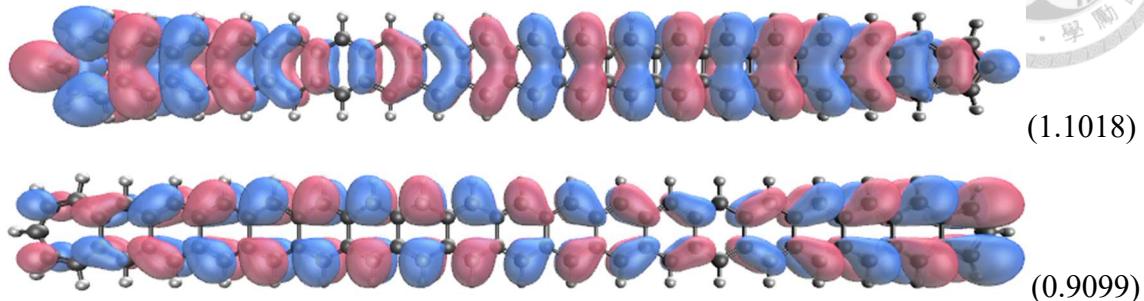


Figure B.14: Real-space representation of HOMO (up) and LUMO (down) for the singlet state of fused azulene-acene ($n=20$) with their occupation number 1.1547 and 0.8589

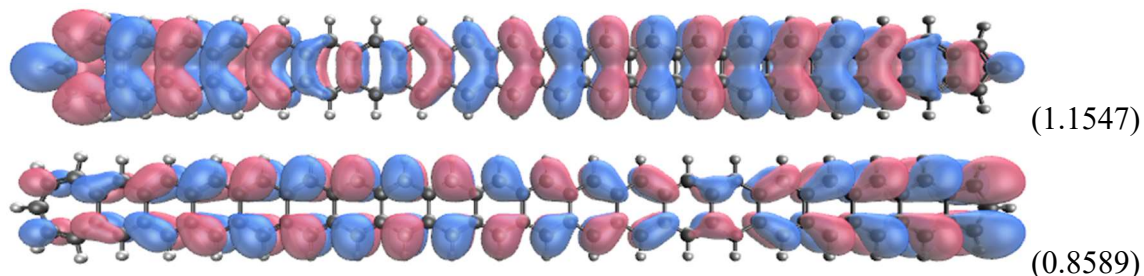


Figure B.15: Real-space representation of HOMO (up) and LUMO (down) for the singlet state of fused azulene-acene ($n=21$) with their occupation number 1.2006 and 0.8146

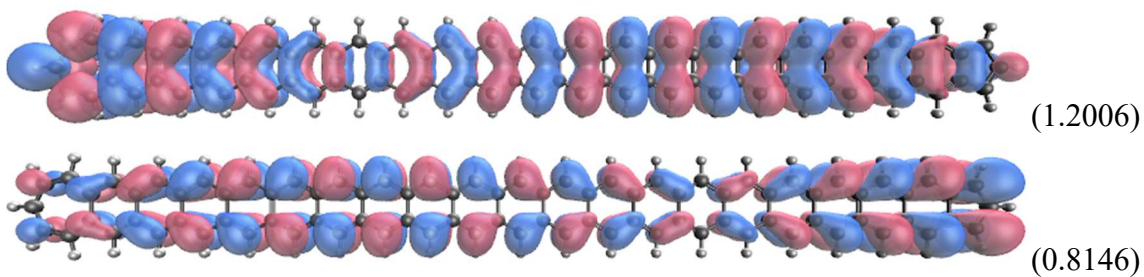


Figure B.16: Real-space representation of HOMO (up) and LUMO (down) for the singlet state of fused azulene-acene ($n=22$) with their occupation number 1.2405 and 0.7761

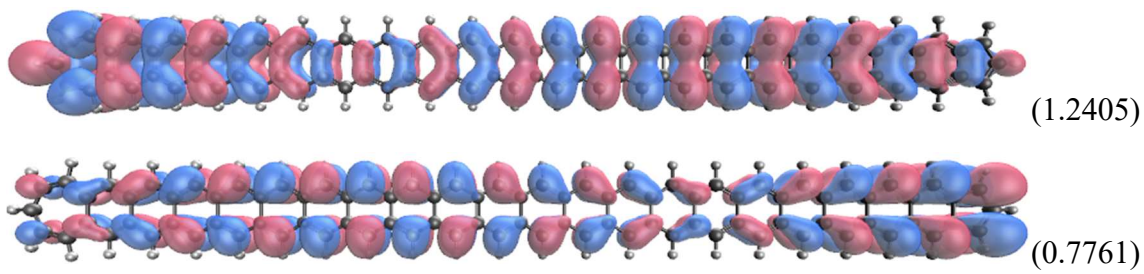


Figure B.17: Real-space representation of HOMO (up) and LUMO (down) for the singlet state of fused azulene-acene ($n=23$) with their occupation number 1.2752 and 0.7426

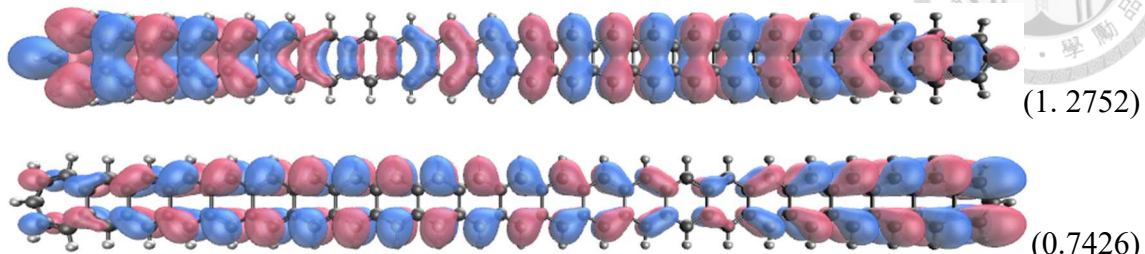


Figure B.18: Real-space representation of HOMO (up) and LUMO (down) for the singlet state of fused azulene-acene ($n=24$) with their occupation number 1.2782 and 0.7158

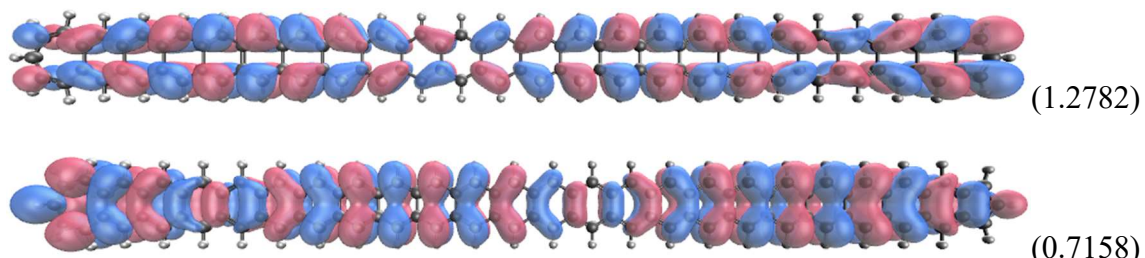


Figure B.19: Real-space representation of HOMO (up) and LUMO (down) for the singlet state of fused azulene-acene ($n=25$) with their occupation number 1.2165 and 0.7807

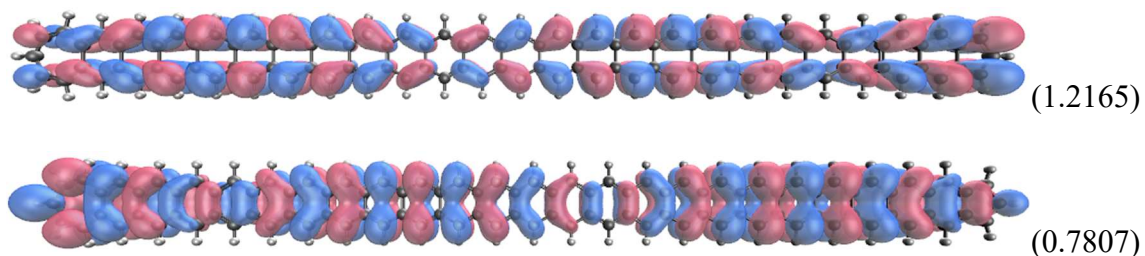


Figure B.20: Real-space representation of HOMO (up) and LUMO (down) for the singlet state of fused azulene-acene ($n=26$) with their occupation number 1.1593 and 0.8409

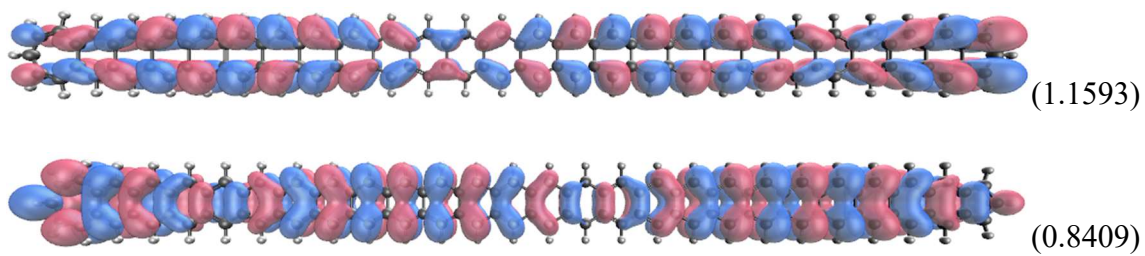


Figure B.21: Real-space representation of HOMO (up) and LUMO (down) for the singlet state of fused azulene-acene ($n=27$) with their occupation number 1.1063 and 0.8967

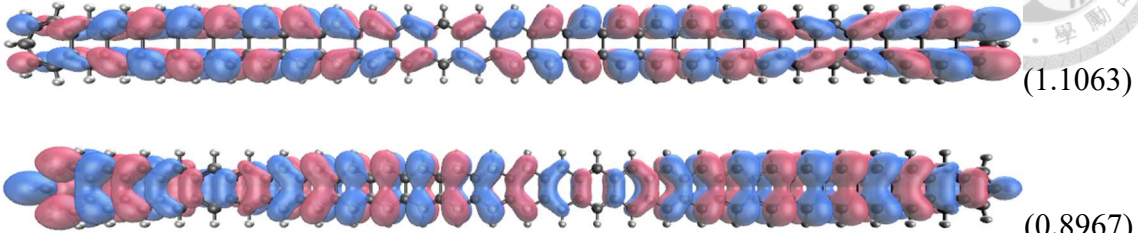


Figure B.22: Real-space representation of HOMO (up) and LUMO (down) for the singlet state of fused azulene-acene ($n=28$) with their occupation number 1.0577 and 0.9478

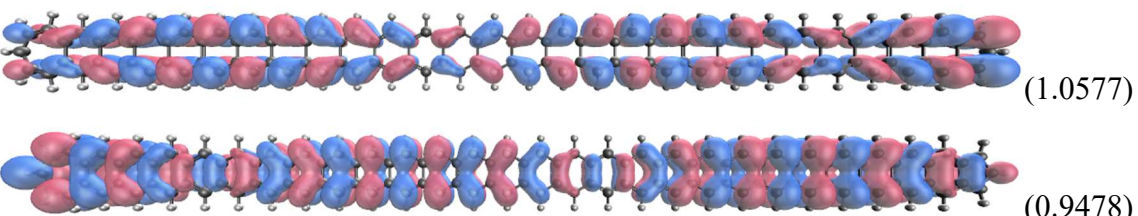


Figure B.23: Real-space representation of HOMO (up) and LUMO (down) for the singlet state of fused azulene-acene ($n=29$) with their occupation number 1.0131 and 0.9948

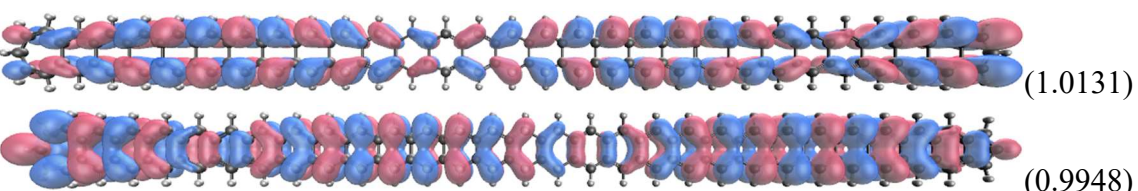


Figure B.24: Real-space representation of HOMO (up) and LUMO (down) for the singlet state of fused azulene-acene ($n=30$) with their occupation number 1.0379 and 0.9721

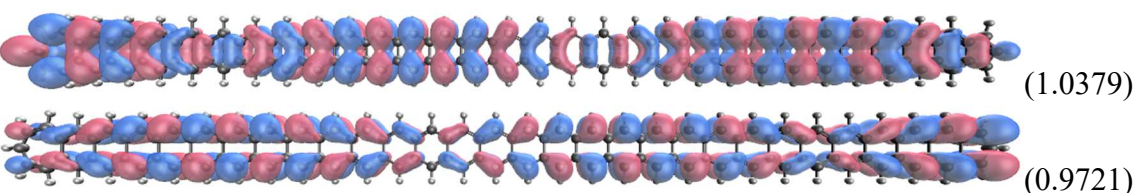


Figure B.25: Real-space representation of HOMO (up) and LUMO (down) for the singlet state of fused azulene-acene ($n=31$) with their occupation number 1.0772 and 0.9347

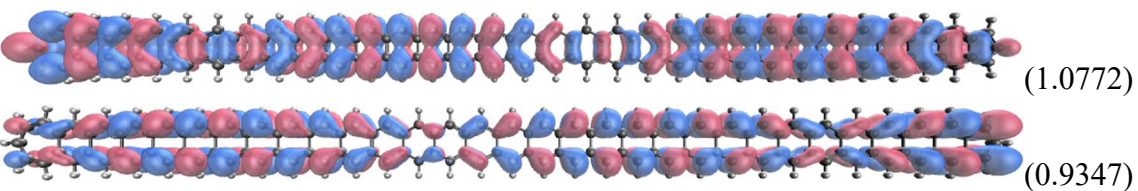


Figure B.26: Real-space representation of HOMO (up) and LUMO (down) for the singlet state of fused azulene-acene ($n=32$) with their occupation number 1.1131 and 0.9004

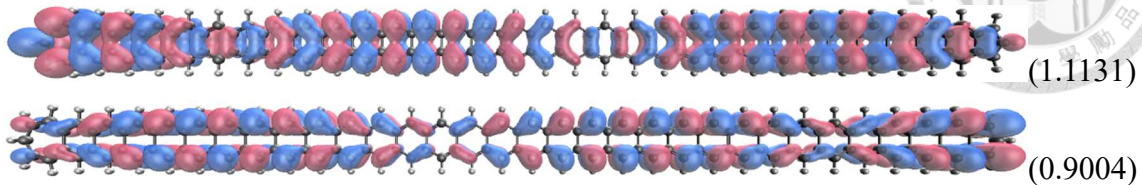


Figure B.27: Real-space representation of HOMO (up) and LUMO (down) for the singlet state of fused azulene-acene ($n=33$) with their occupation number 1.1461 and 0.8690

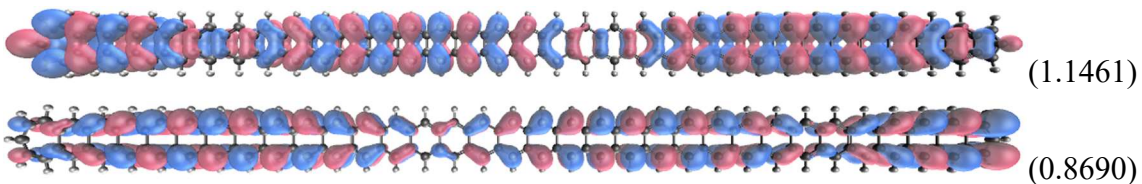


Figure B.28: Real-space representation of HOMO (up) and LUMO (down) for the singlet state of fused azulene-acene ($n=34$) with their occupation number 1.1762 and 0.8402

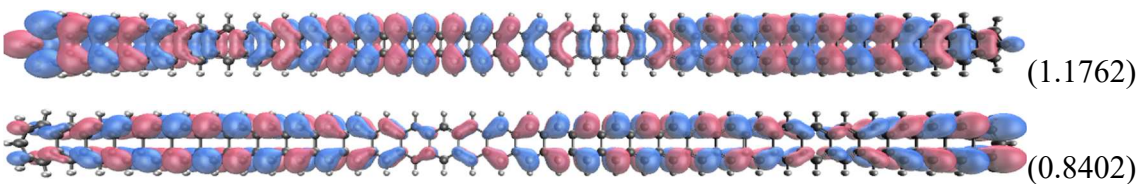


Figure B.29: Real-space representation of HOMO (up) and LUMO (down) for the singlet state of fused azulene-acene ($n=35$) with their occupation number 1.2038 and 0.8138

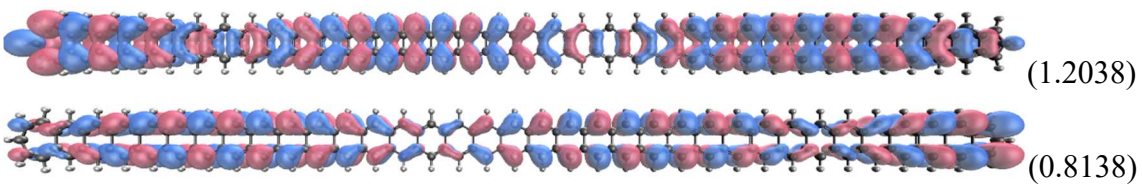
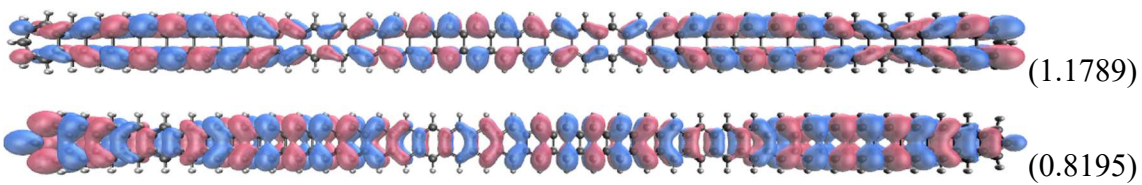


Figure B.30: Real-space representation of HOMO (up) and LUMO (down) for the singlet state of fused azulene-acene ($n=36$) with their occupation number 1.1789 and 0.8195



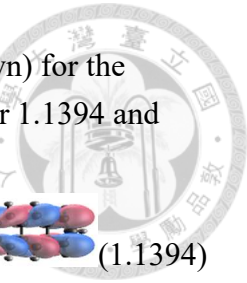


Figure B.31: Real-space representation of HOMO (up) and LUMO (down) for the singlet state of fused azulene-acene ($n=37$) with their occupation number 1.1394 and 0.8614

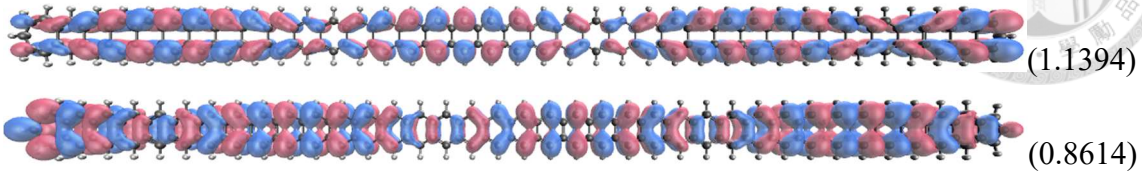


Figure B.32: Real-space representation of HOMO (up) and LUMO (down) for the singlet state of fused azulene-acene ($n=38$) with their occupation number 1.1021 and 0.9008

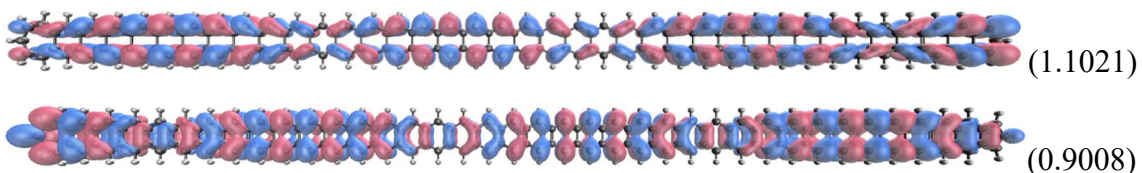


Figure B.33: Real-space representation of HOMO (up) and LUMO (down) for the singlet state of fused azulene-acene ($n=39$) with their occupation number 1.0669 and 0.9380

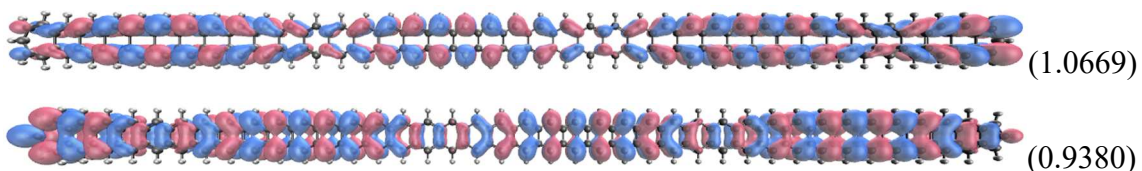


Figure B.34: Real-space representation of HOMO (up) and LUMO (down) for the singlet state of fused azulene-acene ($n=40$) with their occupation number 1.0339 and 0.9730

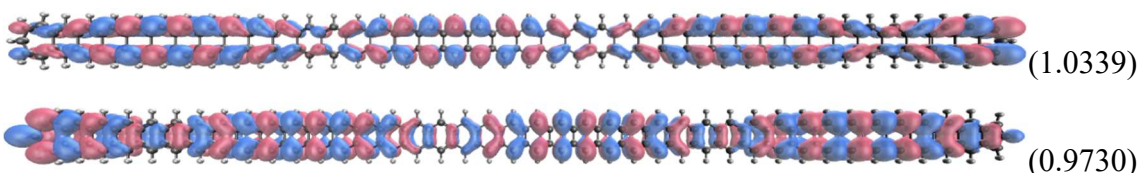


Figure B.35: Real-space representation of HOMO (up) and LUMO (down) for the singlet state of fused azulene-acene ($n=41$) with their occupation number 1.0059 and 1.0027

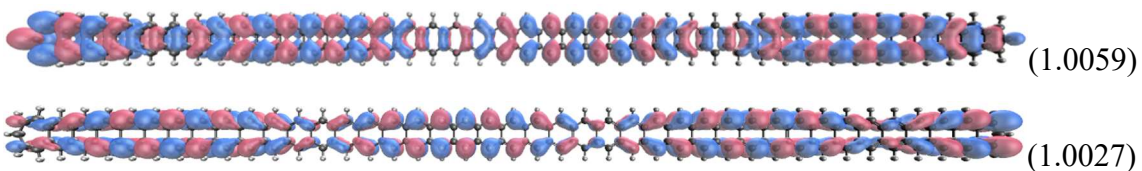


Figure B.36: Real-space representation of HOMO (up) and LUMO (down) for the singlet state of fused azulene-acene ($n=42$) with their occupation number 1.0367 and 0.9736

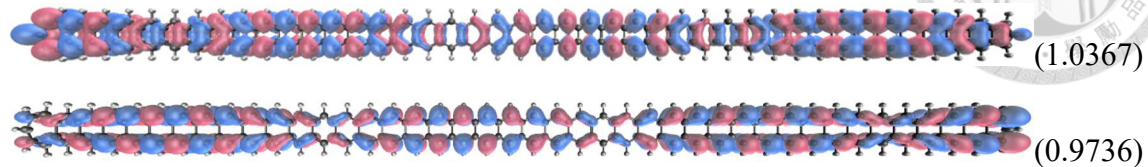


Figure B.37: Real-space representation of HOMO (up) and LUMO (down) for the singlet state of fused azulene-acene ($n=43$) with their occupation number 1.0657 and 0.9462

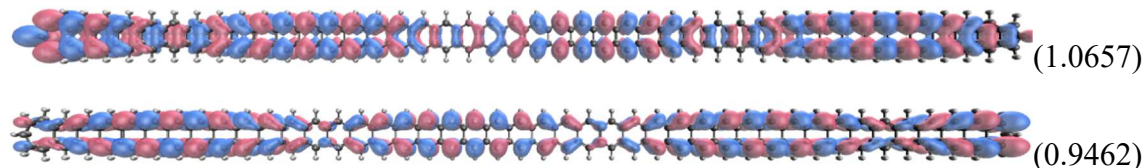


Figure B.38: Real-space representation of HOMO (up) and LUMO (down) for the singlet state of fused azulene-acene ($n=44$) with their occupation number 1.0928 and 0.9204

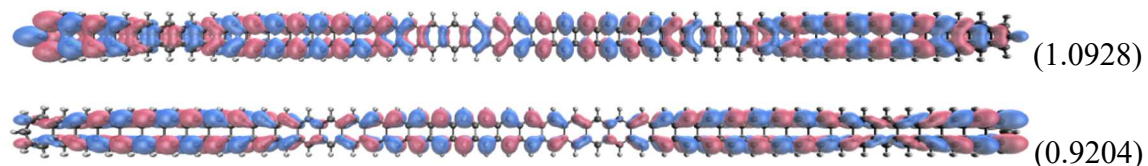


Figure B.39: Real-space representation of HOMO (up) and LUMO (down) for the singlet state of fused azulene-acene ($n=45$) with their occupation number 1.1182 and 0.8963

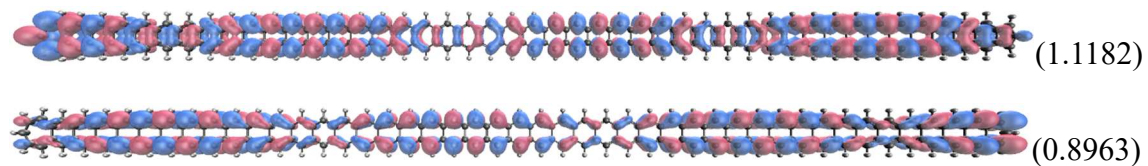
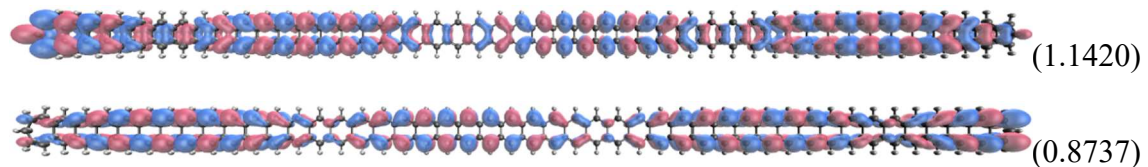


Figure B.40: Real-space representation of HOMO (up) and LUMO (down) for the singlet state of fused azulene-acene ($n=46$) with their occupation number 1.1420 and 0.8737



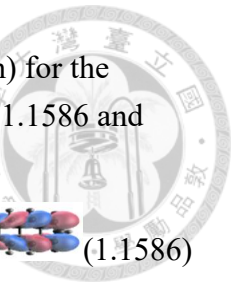


Figure B.41: Real-space representation of HOMO (up) and LUMO (down) for the singlet state of fused azulene-acene ($n=47$) with their occupation number 1.1586 and 0.8523

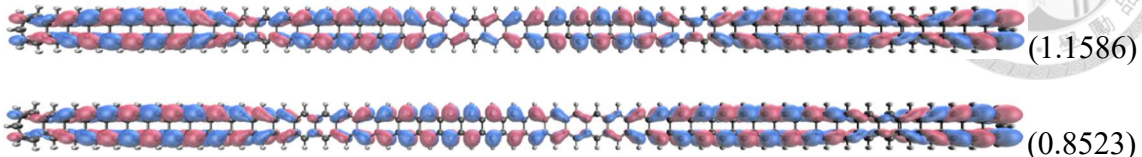


Figure B.42: Real-space representation of HOMO (up) and LUMO (down) for the singlet state of fused azulene-acene ($n=48$) with their occupation number 1.1286 and 0.8725

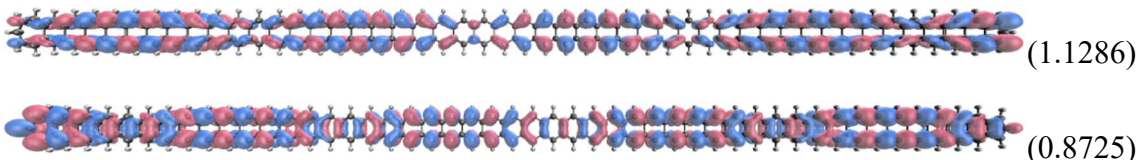


Figure B.43: Real-space representation of HOMO (up) and LUMO (down) for the singlet state of fused azulene-acene ($n=49$) with their occupation number 1.0998 and 0.9031

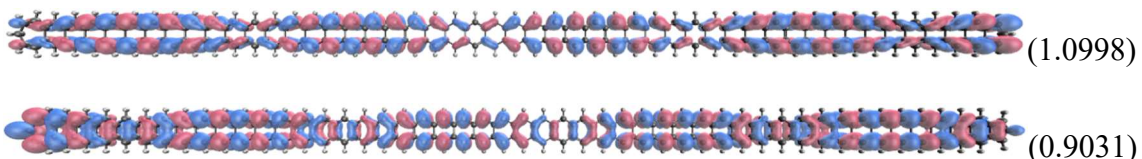


Figure B.44: Real-space representation of HOMO (up) and LUMO (down) for the singlet state of fused azulene-acene ($n=50$) with their occupation number 1.0723 and 0.9323

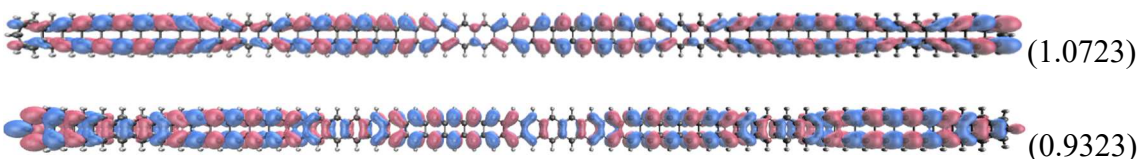


Figure B.45: Real-space representation of HOMO (up) and LUMO (down) for the singlet state of fused azulene-acene ($n=51$) with their occupation number 1.0460 and 0.9601

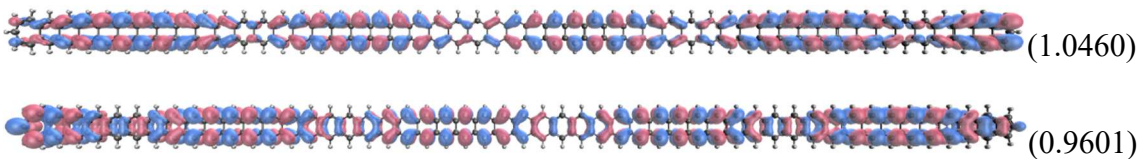


Figure B.46: Real-space representation of HOMO (up) and LUMO (down) for the singlet state of fused azulene-acene ($n=52$) with their occupation number 1.0211 and 0.9866

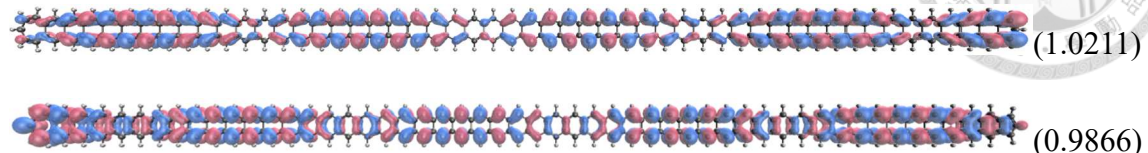


Figure B.47: Real-space representation of HOMO (up) and LUMO (down) for the singlet state of fused azulene-acene ($n=53$) with their occupation number 1.0119 and 0.9972

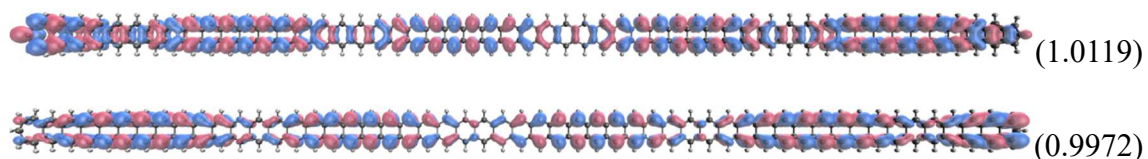


Figure B.48: Real-space representation of HOMO (up) and LUMO (down) for the singlet state of fused azulene-acene ($n=54$) with their occupation number 1.0360 and 0.9745

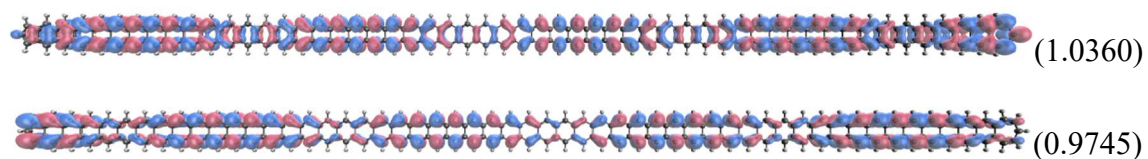


Figure B.49: Real-space representation of HOMO (up) and LUMO (down) for the singlet state of fused azulene-acene ($n=55$) with their occupation number 1.0588 and 0.9529

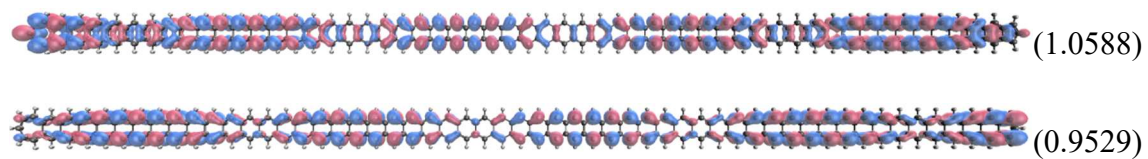


Figure B.50: Real-space representation of HOMO (up) and LUMO (down) for the singlet state of fused azulene-acene ($n=56$) with their occupation number 1.0806 and 0.9323

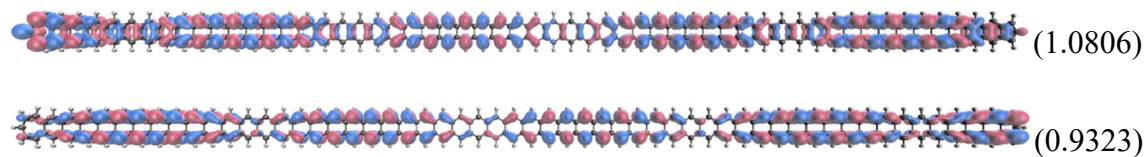


Figure B.51: Real-space representation of HOMO (up) and LUMO (down) for the singlet state of fused azulene-acene ($n=57$) with their occupation number 1.1013 and 0.9127

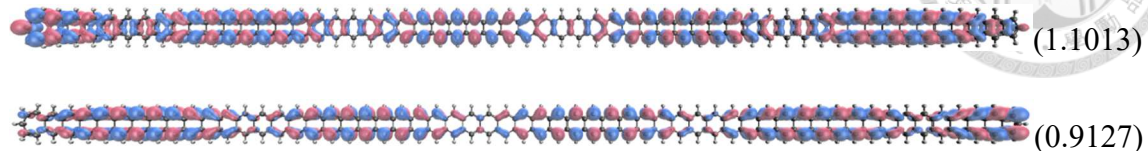


Figure B.52: Real-space representation of HOMO (up) and LUMO (down) for the singlet state of fused azulene-acene ($n=58$) with their occupation number 1.1210 and 0.8941

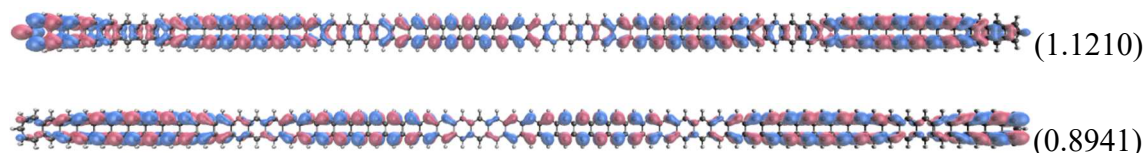


Figure B.53: Real-space representation of HOMO (up) and LUMO (down) for the singlet state of fused azulene-acene ($n=59$) with their occupation number 1.1217 and 0.8797

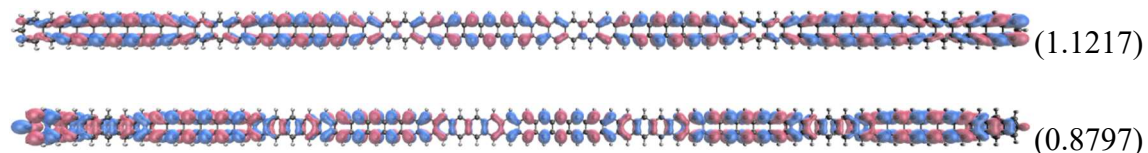


Figure B.54: Real-space representation of HOMO (up) and LUMO (down) for the singlet state of fused azulene-acene ($n=60$) with their occupation number 1.0983 and 0.9046

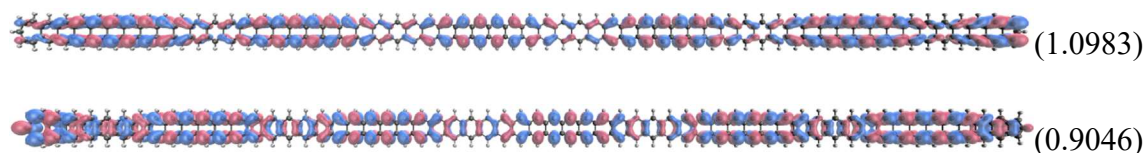
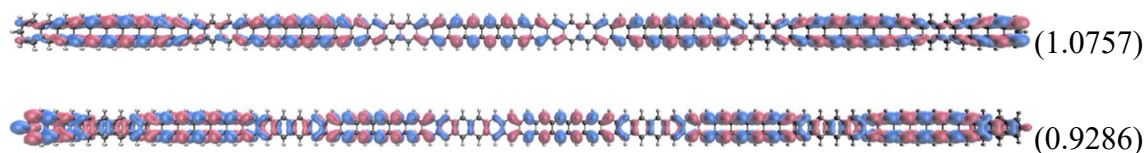


Figure B.55: Real-space representation of HOMO (up) and LUMO (down) for the singlet state of fused azulene-acene ($n=61$) with their occupation number 1.0757 and 0.9286



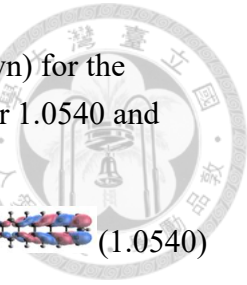


Figure B.56: Real-space representation of HOMO (up) and LUMO (down) for the singlet state of fused azulene-acene ($n=62$) with their occupation number 1.0540 and 0.9517

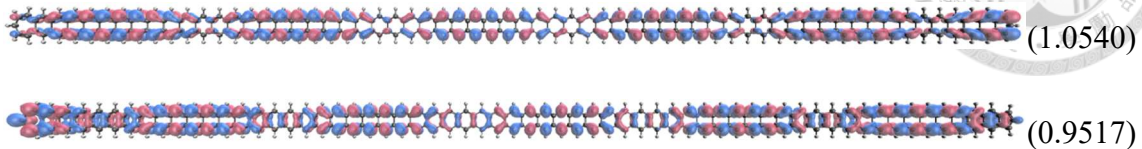


Figure B.57: Real-space representation of HOMO (up) and LUMO (down) for the singlet state of fused azulene-acene ($n=63$) with their occupation number 1.0331 and 0.9740

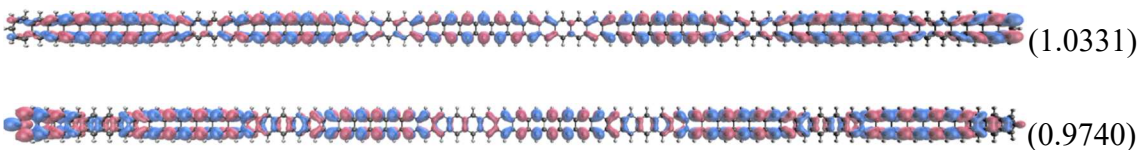


Figure B.58: Real-space representation of HOMO (up) and LUMO (down) for the singlet state of fused azulene-acene ($n=64$) with their occupation number 1.0130 and 0.9953

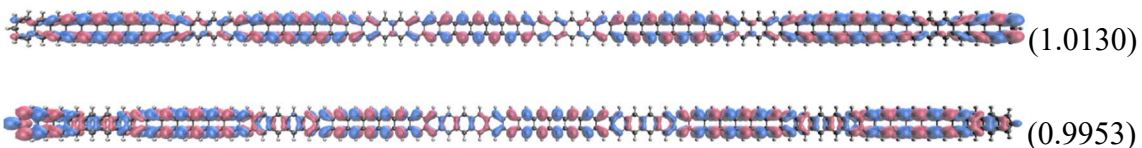


Figure B.59: Real-space representation of HOMO (up) and LUMO (down) for the singlet state of fused azulene-acene ($n=65$) with their occupation number 1.0159 and 0.9936

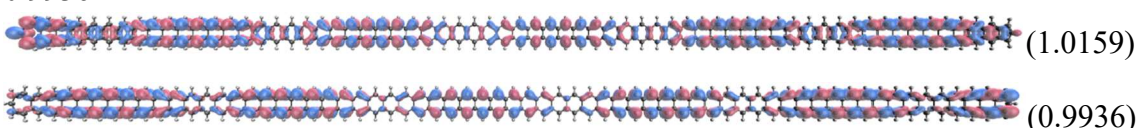


Figure B.60: Real-space representation of HOMO (up) and LUMO (down) for the singlet state of fused azulene-acene ($n=66$) with their occupation number 1.0355 and 0.9750

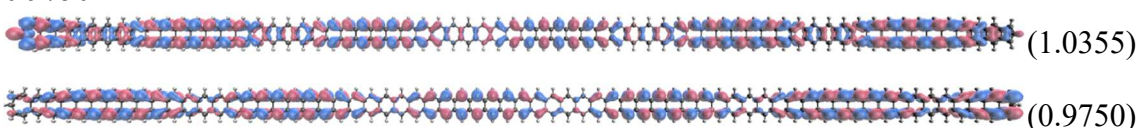


Figure B.61: Real-space representation of HOMO (up) and LUMO (down) for the singlet state of fused azulene-acene ($n=67$) with their occupation number 1.0545 and 0.9572

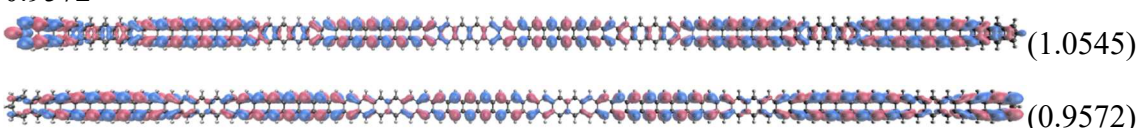


Figure B.62: Real-space representation of HOMO (up) and LUMO (down) for the singlet state of fused azulene-acene ($n=68$) with their occupation number 1.0726 and 0.9401

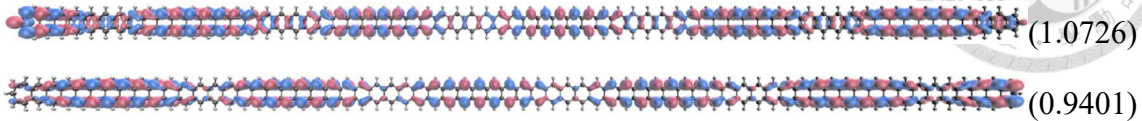


Figure B.63: Real-space representation of HOMO (up) and LUMO (down) for the singlet state of fused azulene-acene ($n=69$) with their occupation number 1.0900 and 0.9236

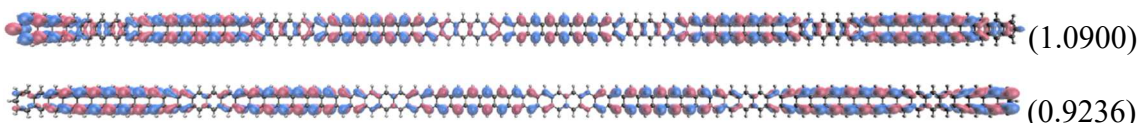


Figure B.64: Real-space representation of HOMO (up) and LUMO (down) for the singlet state of fused azulene-acene ($n=70$) with their occupation number 1.1068 and 0.9078

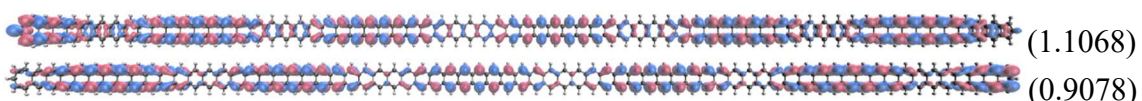


Figure B.65: Real-space representation of HOMO (up) and LUMO (down) for the singlet state of fused azulene-acene ($n=71$) with their occupation number 1.0972 and 0.9057

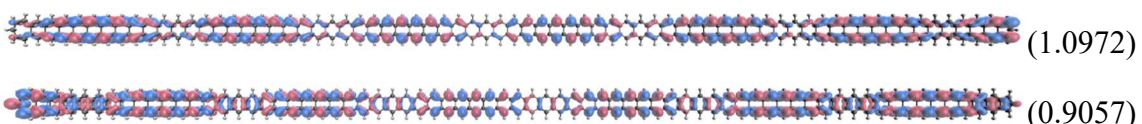


Figure B.66: Real-space representation of HOMO (up) and LUMO (down) for the singlet state of fused azulene-acene ($n=72$) with their occupation number 1.0781 and 0.9261

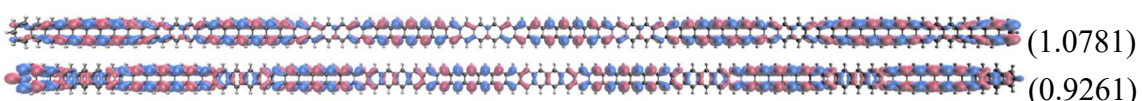


Figure B.67: Real-space representation of HOMO (up) and LUMO (down) for the singlet state of fused azulene-acene ($n=73$) with their occupation number 1.0595 and 0.9458

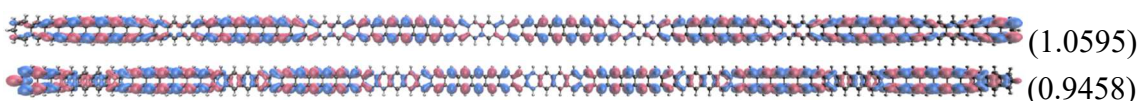


Figure B.68: Real-space representation of HOMO (up) and LUMO (down) for the singlet state of fused azulene-acene ($n=74$) with their occupation number 1.0416 and 0.9649

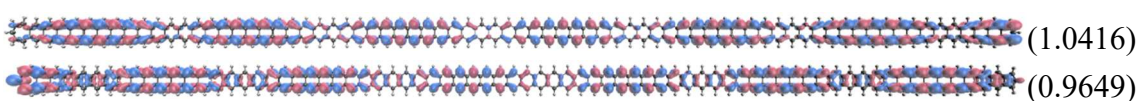


Figure B.69: Real-space representation of HOMO (up) and LUMO (down) for the singlet state of fused azulene-acene ($n=75$) with their occupation number 1.0242 and 0.9834

